Cell Genomics

Article

Microbial single-cell omics *in situ*

Graphical abstract

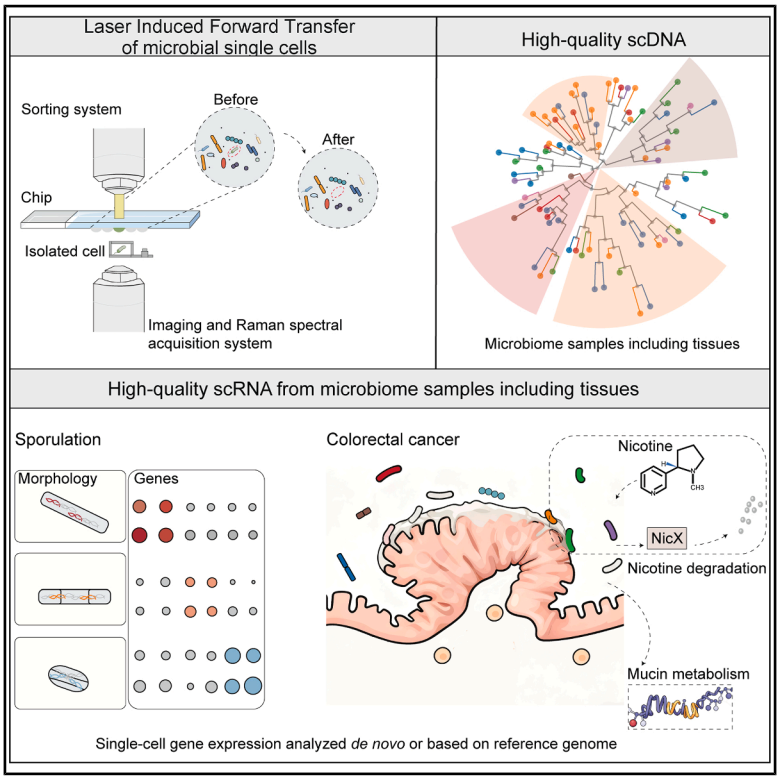

Highlights

- Automated LIFT enables high-quality microbial single-cell genomes or transcriptomes
- Single-cell fate determination is illustrated for sporulation
- Morphology, spectra, or labeling helps maximize the uniqueness of the cells sequenced
- Tissue-resident single microbes were analyzed for colorectal cancer and the mouse gut

Authors

Xihong Lan (蓝希红), Qiaoxing Liang (梁桥星), Jinhua He (何金花), ..., Guoping Zhao (赵国屏), Ruidong Guo (郭瑞东), Huijue Jia (贾慧珏)

Correspondence

huijue_jia@fudan.edu.cn

In brief

Microbial single-cell studies have largely followed the steps of mammalian single-cell technology. Lan et al. develop a laser-based approach where bacterial cells are collected from complex communities or tissue slices and amplified to obtain high-quality single-cell genomes or transcriptomes.

Lan et al., 2026, Cell Genomics *6*, 101128
April 8, 2026
https://doi.org/10.1016/j.xgen.2025.101128

CellPress

Cell Genomics

CellPress
OPEN ACCESS

Article

Microbial single-cell omics *in situ*

Xihong Lan (蓝希红),[1,2,3,4,7] Qiaoxing Liang (梁桥星),[1,2,3,7] Jinhua He (何金花),[4,7] Jiayi Wu (吴嘉仪),[3] Xiaoying Zhang (张小鹰),[4] Fei Li (李飞),[1,2,3] Lili Li (李丽莉),[3] Guoping Zhao (赵国屏),[1,2,5] Ruidong Guo (郭瑞东),[1] and Huijue Jia (贾慧珏)[1,2,3,6,8,*]

[1]School of Life Sciences, Fudan University, Shanghai 200433, China
[2]State Key Laboratory of Genetics and Development of Complex Phenotypes, Fudan University, Shanghai 200433, China
[3]Greater Bay Area Institute of Precision Medicine (Guangzhou), Fudan University, Guangzhou 511458, China
[4]Central Laboratory of Panyu Central Hospital, The Affiliated Panyu Central Hospital of Guangzhou Medical University, Guangzhou 511400, China
[5]Key Laboratory of Systems Health Science of Zhejiang Province, School of Life Science, Hangzhou Institute for Advanced Study, University of Chinese Academy of Sciences, Hangzhou, China
[6]Zhejiang University, Hangzhou, China
[7]These authors contributed equally
[8]Lead contact
*Correspondence: huijue_jia@fudan.edu.cn
https://doi.org/10.1016/j.xgen.2025.101128

SUMMARY

Metagenomics has enabled the understanding of the microbial composition and functional potential in various environments. Using laser-induced forward transfer (LIFT) technology, we report high-quality microbial single-cell genomes or transcriptomes in complex samples such as mouse gut, human saliva, and tumor sections. Bacterial cells in close proximity to each other or to host cells could be directly analyzed using this single-cell approach. Bacterial cells in mice or human samples could be fluorescently labeled for single-cell visualization before collection. The high-quality single-cell transcriptome results allow us to delineate cell-fate commitment in *Bacillus* sporulation and preliminarily characterize gene expression from *Bacteroides* in a colorectal cancer sample. The method is scalable and precise and empowers insights about microbial populations and single-cell interactions with the host.

INTRODUCTION

Single-cell transcriptome analyses of mammalian cells are informing our understanding of the cell types within tissues, and more recently, these insights have been boosted by spatial omics technology.[1] Single-cell omics for bacterial cells have been more difficult to study due to the lower concentration of nucleic acids than eukaryotes, often by orders of magnitude, and the lack of a long poly(A) tail for mRNA amplification (typically over 100 nt in mammalian cells).[2] Moreover, the Poisson distribution of droplet microfluidics lowers the effective number of droplets containing single cells, especially when droplet fusions are required. Marine cyanobacteria were among the first bacteria to be analyzed using single-cell genomes.[3] Single-cell genomes of microbes from extreme environments have revealed genomic features of uncultured bacteria and archaea.[4] Other than low-diversity communities, microbial single-cell studies have mostly been performed in model organisms, such as *Escherichia coli*, and the genome or transcriptome analyzed with targeted methods.[5–9]

Laser-induced forward transfer (LIFT) is a straightforward way of manipulating microparticles, including cells.[10–13] With a laser beam that evaporates or deforms a thin metal coating,[14,15] LIFT is ideally suited for capturing particles in the size range of bacteria (e.g., a typical *E. coli* cell is 2 × 0.5 μm). Fluorescent or isotopic labels could be combined with LIFT to facilitate the selection of cells. With minimum processing of complex samples, LIFT can potentially tolerate objects commonly present in the human microbiome, such as food particles and cell debris, that could undermine analyses using droplet microfluidics.

Metagenomic analyses of low-biomass prokaryotic environments, such as tumors and the placenta, have been costly and controversial.[16] Thus, a direct approach to characterize microbes within tissues composed of over 99.9% host sequences could provide information about bacteria or other microbial cells residing in multicellular eukaryotic hosts.

Here, we present a method to perform microbial single-cell genomic and transcriptome sequencing using commercially available optics equipment, demonstrating their utility in a number of scenarios, from single-cell heterogeneity in pure culture to complex host microbiome samples and tissue slices.

RESULTS

Draft genome quality assembly for microbial single cells

LIFT-based equipment has recently been devised and optimized.[17] We applied LIFT to human microbiome samples such as urine, saliva, feces, and soil (STAR Methods; Figures S1A–S1D; Video S1). The energy of the laser beam used, and consequently the laser spot size, of LIFT is

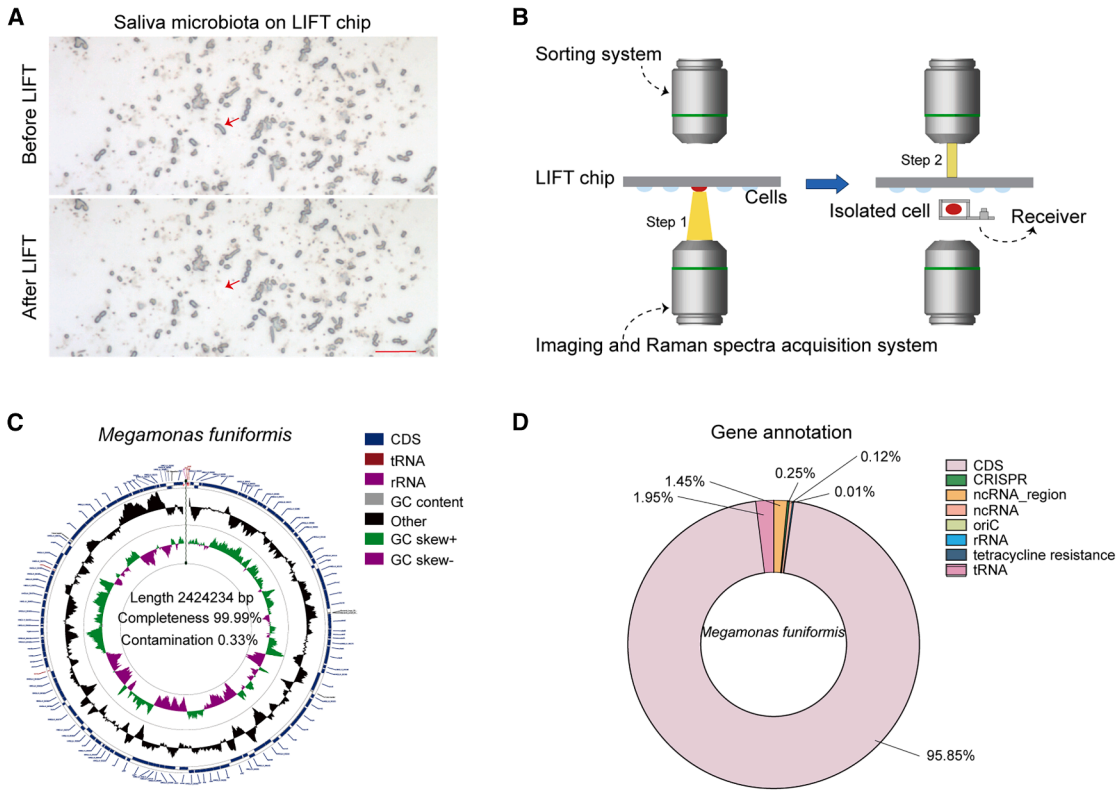

Figure 1. High-quality microbial single-cell draft genome obtained from saliva

(A) Images of saliva microbiome samples before and after LIFT ejection. A single cell, indicated by a red arrow, was LIFTed for genomic sequencing. Scale bar, 10 μm.

(B) Diagram illustrating the steps of image capture, Raman spectra acquisition, and single-cell isolation. In step 1, Raman spectra acquisition and image capture of individual microbial cells were achieved by an inverted microscope (imaging and Raman spectra acquisition system of the commercially available PRECI SCS-R300 equipment). In step 2, a laser from an upright microscope (sorting system) sorts microbial single cells on the chip. The receivers are placed on a wheel, whose rotation is controlled by the manufacturer's software (multiple cells could also be transferred into the same collector, depending on the experimental design).

(C) Visualization of single-cell assembled genome (*Megamonas funiformis*) by the CGView tool displaying GC skew (green and purple, inner ring), GC content (dark gray), feature labels (located on the outermost ring), divider rings, and tick density. A positive GC skew (G > C) is shown in green, while a negative GC skew (G < C) is shown in purple. The outermost ring shows features of the genome including the coding sequence (CDS, blue) and tRNA (red), rRNA, etc. Divider rings (gray circles) are used to separate different data layers and are typically placed between these layers. Tick density indicates positions along the genome. The line at the top of the Circos plot is the sequence ruler itself—a coordinate axis that starts at the 12-o'clock position of the circle and runs clockwise, marking the direction of the coding strand, and the position of 16S ribosomal RNA (*rrf*), tRNA (*trnH*, *trnW*, and *trnS*).

(D) The pie chart of a single-cell assembled genome annotation (*M. funiformis*) displays different categories, including CDS, CRISPR, ncRNA region, ncRNA, replication origin (oriC), rRNA, tetracycline resistance, and tRNA, with their respective proportions.

adjustable (Figures S1A, S1B, and S2). We explored the energy and mode required for microbial cell ejection using bacteria of different sizes and shapes, including *Staphylococcus capitis*, *Lactobacillus plantarum*, *Akkermansia muciniphila*, *Streptococcus oralis*, and *Clostridium butyricum*, which range in size from 0.5 to 9.4 μm (Figure S2). Low energy from the laser (< ~40 nJ) resulted in cell ejection failure, including cell shifting and cell rupture (Figures S2A and S2B), while appropriate energy for cell ejection successfully isolated the selected cell without affecting closely adjacent cells (Figure S2C). The separation of cells with different morphological characters suggests that the appropriate energy for bacterial single-cell LIFT was related to the size of the cell rather than its shape (Figure S2D). Yet, bacterial cells in an elongated shape could require multiple LIFT attempts, without increasing the energy of individual shots (Figure S2E).

To develop microbial single-cell technology for complex samples, we started with saliva samples from adult humans, which could contain hundreds of species (Figure S3A). A fresh saliva sample was centrifuged and spotted onto the slide (Figure S1C), and bacterial cells were visualized before LIFT (Figure 1A). Single cells were ejected by LIFT without affecting neighboring cells (Figures 1A and 1B, no burnt circle with a low energy of 60 nJ), and multiple displacement amplification (MDA) was performed in a PCR tube. Without the need for sophisticated algorithms to pool assembly from fragmental genomes, as reported,[5] we used state-of-the-art algorithms developed for metagenomes[18] and obtained a bacterial genome

of 99.99% completeness and 0.33% contamination (Figures 1C and S3B–S3E). This genome was identified as *Megamonas funiformis*. Gene annotation through Bakta revealed coding sequences (CDSs), tRNAs, rRNAs, non-coding RNAs (ncRNAs), and CRISPRs (Figure 1D; Table S1). Calculating the coding density showed that the genome sequence is >90% coding (Figures S3F–S3G), which is within the range for commensal bacteria (which averages 87% for human gut[19]). Other oral-resident bacteria, such as *Neisseria sicca* B and *Streptococcus salivarius*, also yielded similarly high-quality single-cell assembled genomes (SAGs) (Figures S3I and S3J). Thus, LIFT from complex samples could obtain high-quality single-cell bacteria genomes (SAGs) that exceed the quality of typical single-cell genomes[5] or metagenomically assembled genomes[20] and are on par with genomes from cultured isolates.

To validate the image- or label-based selection and automated ejection process enabled by the equipment manufacturer, we used *Sphingomonas* sp000797515 fluorescently labeled with tetramethylrhodamine-amino-D-alanine (TADA). Cells were precisely ejected from sparse regions and densely packed regions in a mixture of several species, confirming the spatial precision of this approach (Figures S4A and S4B; Video S2). The *Sphingomonas* sp000797515 cells were sequenced using two different reaction volumes, both of which yielded high-quality genomes (Figures S4C–S4F; Video S2). The smaller volume represents a first step in lowering reagent costs for future applications (Figures S4C and S4D; Table S2). There were no significant differences in genome completeness, contamination, and coverage between the genomes obtained by the two volumes, indicating that downsizing the reaction volume does not lead to a decline in SAG quality (Figure S4E). The single-cell genomes from LIFT were also highly consistent (average nucleotide identity [ANI] > 95%) with the known input genomes (Figure S4F), validating this approach.

To increase the throughput and eliminate individual differences in operation, we used an automated pipetting platform after the automated single-cell ejection. With the aid of automatic identification by adjusting parameters such as diameter, area, and fluorescence intensity, 34–62 bacteria from single-strain suspensions and complex samples could be precisely ejected and collected within 1 min (Figures S5A–S5C; Videos S3 and S4). Salivary microbes of three views from a single sample were marked for collection (0.1 s per cell), which consisted of diverse morphological characters (Figure 2A). After *de novo* assembly, 4 of the 39 SAGs showed a completeness of >90% and a contamination of <5%, which are regarded as high quality.[21] 27 of the 39 SAGs showed >50% completeness and <10% contamination, which are medium quality (Table S3). Species were identified according to GTDB-Tk with ANI > 95%. This relatively small-scale sampling obtained oral bacteria from all expected major phyla, including Actinobacteriota, Bacteroidota, Campylobacterota, Firmicutes, Fusobacteriota, Patescibacteria, and Proteobacteria (Figure 2B). Species from the oral cavity and related body sites were sampled, including *Nanosynbacter lyticus* TM7x, *Haemophilus* sp., *Neisserria* sp., *Porphyromonas gingivalis*, *Filifactor alocis*, *Fusobacterium peridonticum*, *Bifidobacterium vaginale* (renamed from *Gardnerella vaginalis*), and *Parabacteroides merdae* (Figure 2B). These results indicate that the single-cell genomes could be reliably obtained with medium- to high-quality sequencing in an automated and selective manner to reveal the microbial landscape in a complex sample.

Cell-fate commitment revealed by single-cell transcriptome

Sporulation is a strategy allowing bacteria to survive harsh environments[22,23] and to potentially be distributed to other hosts. We cultured a strain of *Bacillus licheniformis* isolated from human saliva, added citric acid to the *B. licheniformis* culture to induce sporulation over 9 days, and LIFT-picked single cells to analyze their transcriptome (Figure S6A). Hundreds to thousands of transcripts were detected from cells stimulated by citric acid (Figure S6B), consistent with widespread yet incomplete expression of the bacterial genome per cell cycle, such as that known for *E. coli*.[24] Besides protein-coding genes, tRNAs and regulatory small RNAs (sRNAs) were also detected (Figure S6C), demonstrating the robustness of the experimental protocol.

In addition to single-cell RNA (scRNA) analysis based on the *B. licheniformis* reference genome (Figures S6D–S6G), the high-quality reads obtained could be *de novo* assembled. Gene counts obtained by a reference-based and *de novo* (reference-free) approach were significantly similar ($p < 0.05$), and the expression profile was highly correlated (Figure S6H). Thus, both known and unknown bacteria could be investigated using this scRNA approach, a key advantage compared to FISH (fluorescence *in situ* hybridization).

Oligo(A) tails target bacterial mRNAs for degradation.[25] This coupling to exonucleases in bacteria is evolutionarily similar to exosome degradation of transcripts in the eukaryotic nucleus. We detected stretches of three or more adenylates in a number of transcripts (Figures S7A–S7F; Table S4). *TctA* (tripartite tricarboxylate transporter TctA family), a large transmembrane protein involved in citrate uptake, for example, showed long stretches of poly(A) spanning the entire gene, which had three contigs in *de novo* assembly (Figures S7G–S7I). The shorter form was more abundant in five of the five cells analyzed (Figure S7H), consistent with degradation from 3′ to 5′. These results highlight the single-nucleotide resolution of our microbial single-cell transcriptome data and caution against methods that add a long poly(A) tail for amplification[2,9] if such RNA dynamics are being investigated.

We next explored the dynamic transcription changes during the commitment to sporulation in *B. licheniformis* following citric acid treatment. In addition to the upright laser for LIFT, the equipment we used also harbor an inverted laser for single-cell Raman spectrometry (Figures 3A and S1A). Both the cell morphology and Raman spectra could be rapidly obtained from a sample, before or without LIFT. During citric-acid-induced sporulation, day 0, 3, and 9 *B. licheniformis* cells could be visually and spectrally divided into three groups: day 0 rod (group α), day 3 intermediate state (group β), and day 9 oval spore (group γ) (Figure 3A). Spectra from the individual microbial cells formed three clusters (Figure 3B), and the mean spectra of α, β, and γ cells were different (Figures 3B and 3C). The morphological features of bacteria, as well as the Raman spectra, suggested alterations in cellular gene expressions. Consistent with the decrease in growth during sporulation, while ribosomal RNAs, ribosomal proteins, and

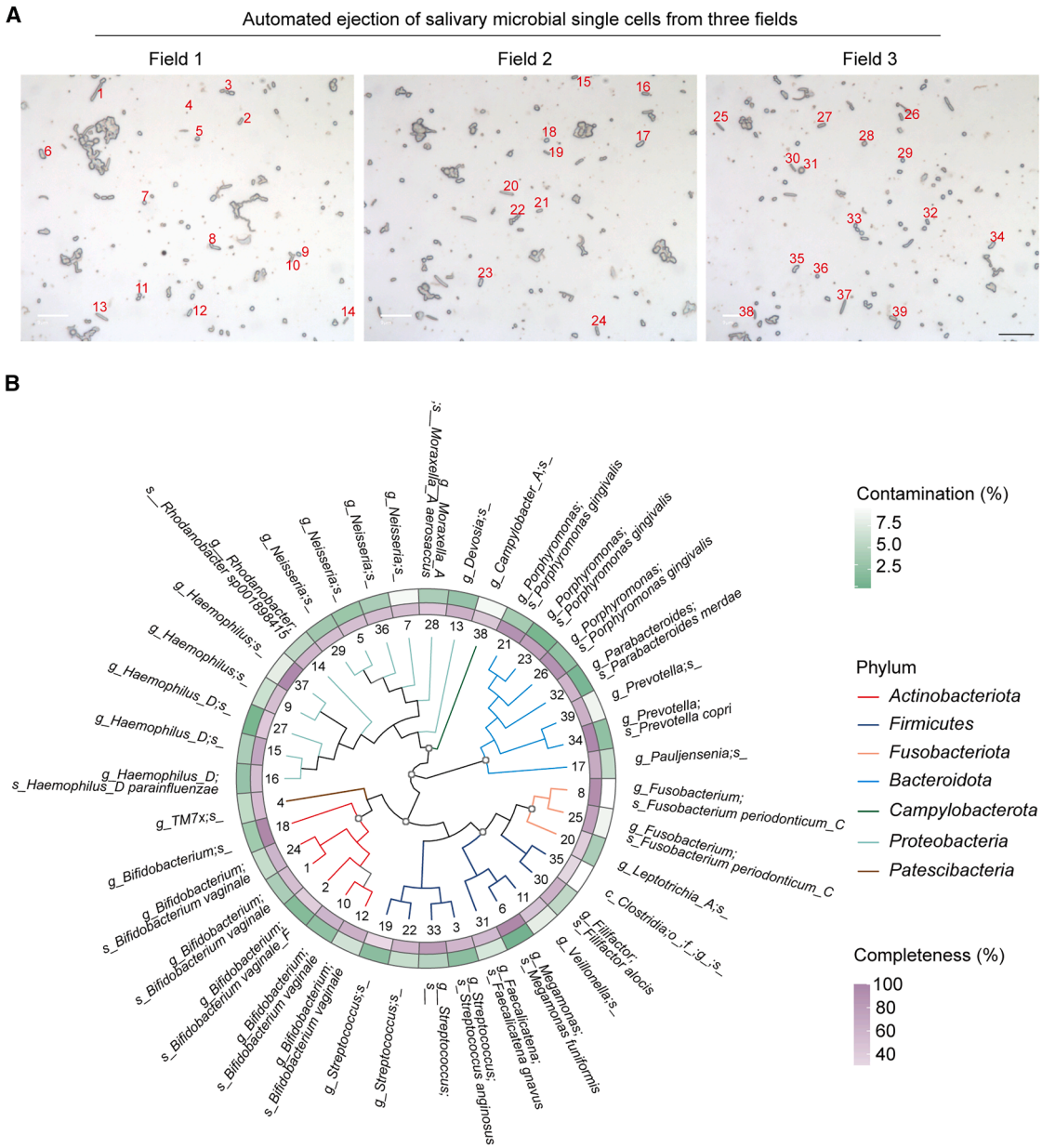

Figure 2. Automated microbial single-cell genomics

(A) Individual microbial cells of saliva distributed on the chip were observed before LIFT. The selected microbial single cells with variable morphology from three fields, numerically marked with red, are ejected for single-cell sequencing. The red numbers are next to the ejected cells, above or to the right. This is a feature offered by the equipment manufacturer's software (Video S4). Scale bar, 10 μm.

(B) A phylogeny constructed from 39 obtained SAG sequences (PhyloPhlAn, maximum likelihood) is represented by the inner dendrogram. The phylum of each SAG is indicated by the branch color. The cell numbers indicated on the branches correspond to the cell numbers shown in (A), so the single-cell morphology can be matched with the single-cell genome. The completeness (purple) and contamination (green, inverse scale) of each SAG are represented by two heatmaps overlaid on the phylogenetic tree. The species name of each SAG is listed in the outermost ring.

nucleoid-associated proteins dominated the day 0 transcriptome, the proportion of reads of other genes notably increased as the cells underwent morphological changes toward sporulation (Figure S8A).

Comparison of the gene expression of α, β, and γ cells allowed us to identify 194 differentially expressed genes, which clustered into three groups that corresponded to higher expression in the α, β, and γ cells, respectively (Figure 3D). Gene Ontology (GO) analysis of the biological process, molecular function, and cell component showed that the genes preferentially expressed in the intermediate state of group II are linked to pathways such as the cellular response to stress,

CellPress
OPEN ACCESS

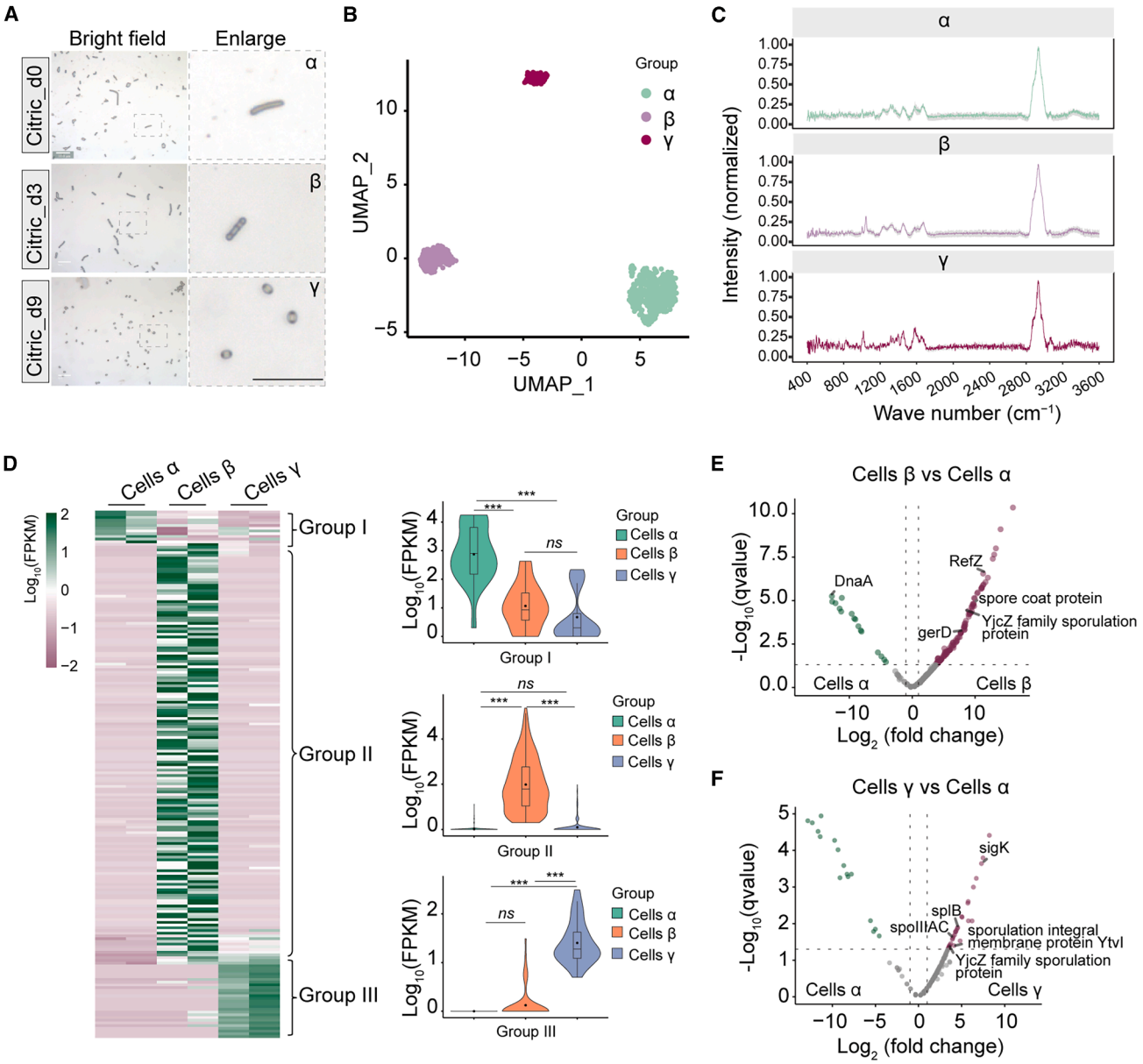

Figure 3. Coherent grouping of sporulating *B. licheniformis* cells visually, spectrally, and with the scRNA transcriptome

(A) Individual *B. licheniformis* α (treated without citric acid), β (treated with citric acid for 3 days, showing compartmentalization), and γ (treated with citric acid for 9 days, spherical or oval shape) cells distributed on the chip were observed in the bright field before Raman spectral acquisition and LIFT ejection. Scale bar, 10 μm.

(B) More than 50 cells from each group (α, β, and γ cells) are selected for Raman spectral acquisition. Dimensionality reduction is performed on the obtained Raman spectra by UMAP.

(C) Display of average Raman spectra (colored) for α, β, and γ cells. The means (green or magenta line) and standard deviations (gray shade) of Raman spectra were calculated for each group. The Raman spectra were normalized to the intensity of the strongest feature in each spectrum.

(D) *B. licheniformis* of α (treated without citric acid), β (treated with citric acid for 3 days), and γ (treated with citric acid for 9 days) morphological forms were ejected (two cells for each group) for scRNA sequencing. A heatmap of differentially expressed transcripts (log-transformed FPKM values) in α, β, and γ cells is shown. The candidate transcripts are mainly clustered into three groups (left). The violin and boxplots show normalized transcript expression in groups I, II, and III (right). ***$p < 0.001$ was determined by two-way analysis of variance (ANOVA). The boxplots indicate the 25th percentile (bottom of the box), median (horizontal yellow line inside the box), mean value (dark spot inside the box), and 75th percentile (top of the box). Whiskers indicate 1.5 times the interquartile range. FPKM, fragment per kilobase of transcript.

(E) Volcano plot of differentially expressed genes of β versus α cells. Gene expression and gene fold change were analyzed and compared by DeSeq2.

(F) Volcano plot of differentially expressed genes of γ versus α cells. Gene expression and gene fold change were analyzed and compared by DeSeq2.

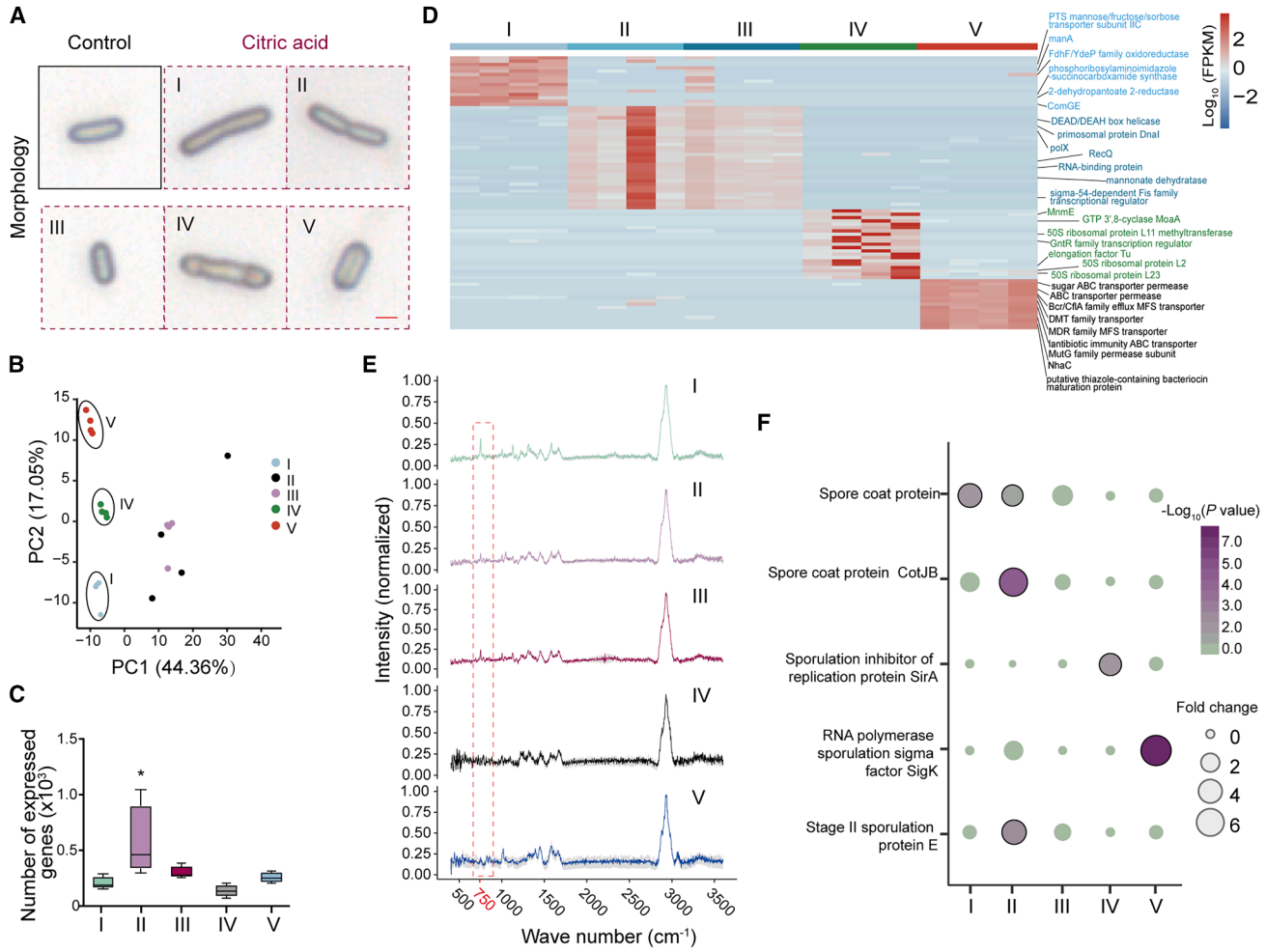

Figure 4. Single-cell transcriptome reveals heterogeneity in sporulation

(A) Representative images of *B. licheniformis* cells with five different morphologies in samples treated with citric acid for 3 days and cells without citric acid treatment as control. Morphologically, type I cells are elongated rod-shaped cells that appear upon acid stimulation; type II cells are marked by a slight constriction or indentation at the center of the cell; type III cells are short rod-shaped cells, typically half the length of type II cells; type IV cells show compartmentalization as a sign of spore formation within the cells; and type V cells are characterized by a spherical or oval shape and a smaller size, consistent with mature spores (group γ in Figure 3). Ten cells were examined for each morphology. Scale bar, 1 μm.

(B) Principal component analysis of the scRNA gene expression profiles from the five cell types (four cells for each type).

(C) Calculation of the number of genes detected in each cell type (4 cells in each type, as in B). Data are represented as the mean ± SE (*$p < 0.05$, **$p < 0.01$, and ***$p < 0.001$) and were calculated using a two-tailed unpaired Student's t test.

(D) Heatmap of representative gene expression (Z score of log-transformed FPKM values) from a total of 20 individual *B. licheniformis* cells (four cells for each type) grown in day 3 citric-acid-treated media. FPKM, fragment per kilobase of transcript.

(E) Raman spectra of five type *B. licheniformis* cells. The colorful spectra are averages of ten individual spectra and normalized to the intensity of the strongest feature in each spectrum. One standard deviation is shown in gray.

(F) Dot plot of genes involved in *B. licheniformis* sporulation. The gene expression (fold change) and p value were calculated between the selected cell types and compared to the remaining cell types. The color gradient reflects the magnitude of the p value, whereas the size of the dot corresponds to the gene fold change.

sporulation, hydrolase activity, and the intrinsic component of membrane (Figure S8B). Consistently, electron microscopy confirmed that cellular component assembly occurred in β cells (Figure S8C), which was also observed under the microscope in the LIFT device (Figure 3A). Comparing α and β cells, we found that the germination gene *gerD*, together with sporulation-related genes, such as spore coat protein and *YjcZ* family sporulation protein, was upregulated after citric acid treatment at day 3 (Figure 3E). When α cells transformed into spores, *spoIIIAC* (stage III sporulation protein AC), *YtvI* (sporulation integral membrane protein), and spore-specific gene *splB* (spore photoproduct lyase) were highly expressed (Figure 3F).

Further looking into the day 3 samples led to five types of cells with distinct cell morphology (Figure 4A). scRNA gene expression profiles showed clear separation on the 2nd principal component for the cells of types I, IV, and V (Figure 4B). Uniform manifold approximation and projection (UMAP) analysis was also performed on the cells (Figure S8D). Comparing gene

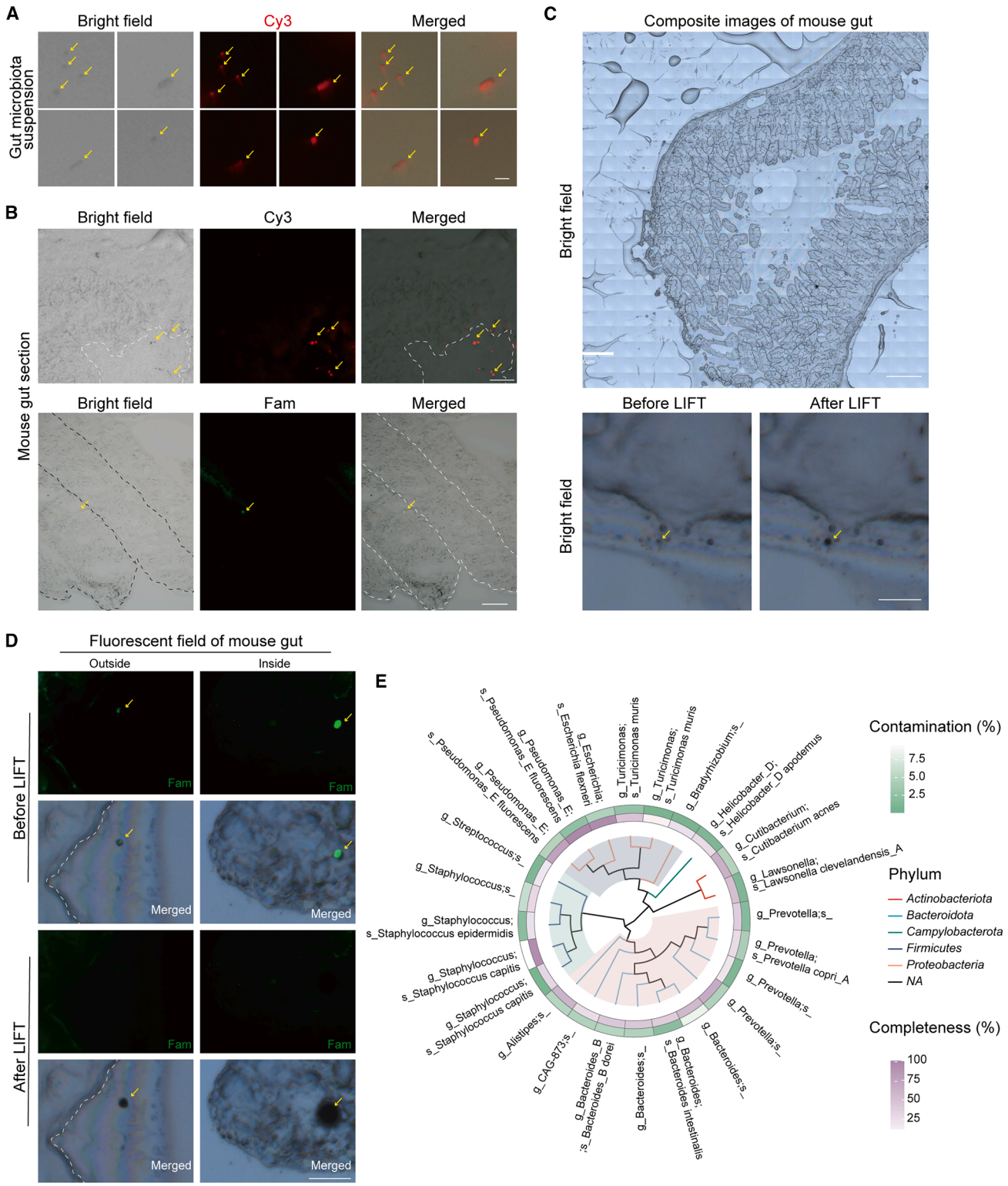

Figure 5. LIFT ejection of bacteria in mouse gut in bright and fluorescent fields

(A) Representative images of bacterial morphology in mouse large intestinal lavage suspension after gavage with Cy3-ADA in mice (n = 3). Scale bar, 10 μm.

(B) Cy3-ADA and Fam-ADA labeled bacteria on mouse gut sections (marked by arrows). Scale bar, 100 μm.

(C) Localized composite image of mouse large intestinal tissue sections (top). Scale bar, 200 μm. LIFT ejection of bacteria on mouse gut sections in the bright field (bottom). Scale bar, 10 μm.

(legend continued on next page)

counts in each type, we found that cells of type II in the cell division state were still active in gene transcription (Figure 4C), and this type of cell decreased in number during the first 3 days of citric acid treatment (Figure S8E). Type IV cells, on the other hand, increased during days 2–4.

Genes whose expression was enriched in the different cell types included enzymes, transcription regulators, and biosynthesis proteins (Figure 4D). Genes highly expressed in type I cells include *FdhF/YdeP* family oxidoreductase,[26] *manA* (mannose-6-phosphate isomerase, class I),[26] PTS mannose/fructose/sorbose transporter subunit IIC,[27] phosphoribosylaminoimidazolesuccinocarboxamide synthase,[28] *ComGE*,[29] and 2-dehydropantoate 2-reductase,[30] which likely confer type I cells with resistance to low pH (citric acid), transporting sugar molecules, pantothenate biosynthesis, DNA uptake, and purine biosynthesis.[26–30] Genes highly expressed in type II cells included DEAD/DEAH-box helicase, primosomal protein DnaI, DNA polymerase/3′-5′ exonuclease PolX, DNA helicase RecQ, RNA-binding protein, and sigma-54-dependent Fis family transcriptional regulator, which indicate that cells are undergoing cell division and ongoing DNA replication and gene transcription processes.[31,32] Genes observed in type II cells were also expressed in type III cells (Figure 4D). When cells changed into type IV cells, GTP-associated genes *MnmE*, elongation factor Tu, and GTP 3′,8-cyclase *MoaA*, 50S ribosomal proteins, and the *GntR* family transcriptional regulator were highly expressed, which regulate biological processes such as gene translation and cell motility.[33,34]

Genes in type V cells were mainly transporters, Na+/H+ antiporter *NhaC*, permease, and bacteriocin, which functioned in stress resistance, substance exchange, and inhibition of spore germination.[35–37] Comparing the mean Raman spectra of the five types of cells, we observed a Raman signal at band 750–785 nm, most likely due to the decrease in cytochrome *c* and metabolites of purine degradation (Figure 4E)[38,39] with sporulation. In addition, transcription of sporulation and spore-related genes also varied among the five types (Figure 4F). These results illustrate the discovery power of high-quality scRNA and indicate that visual and/or label-free Raman spectra-guided selection of microbial single cells could facilitate the investigation of heterogeneous microbial populations and reduce the number of cells sequenced. All cells could be rapidly scanned in seconds, before more costly amplification and analyses, as is typical of microfluidics-based approaches (Table S5).

Single-cell microbial genome and transcriptome from tissue-resident microbiota *in situ*

Having demonstrated single-cell draft genomes from complex samples and high-quality precision single-cell transcriptomes from heterogeneous populations, we directly studied microbial single cells in tissue samples, which has not been previously possible. D-amino acids are essential components of the bacterial peptidoglycan cell wall, and fluorescent D-amino acids can be used for labeling bacteria both *in vivo* and *in vitro*.[40] Here, we used D-amino acids to fluorescently label live bacterial cells in tissue slices. After gavage of mice with fluorescently labeled amino acids (Cy3-amino-D-alanine [Cy3ADA] and Fam-amino-D-alanine [FADA]), various morphologies of bacteria were observed in intestinal lavage fluid (Figure 5A). We observed fluorescent bacteria near the mucus of a mouse colon and inside host cells (Figure 5B). Single bacteria could be extracted from these regions either in a fluorescence-dependent or -independent manner (Figures 5C and 5D). We selected 25 bacteria from three fields for genome sequencing, obtaining 25 SAGs including 3 high-quality and 5 medium-quality genomes. Among these bacteria, we observed typical mouse gut bacteria such as *Prevotella copri* A, *Escherichia flexneri*, *Turicimonas muris*, *Bacteroides intestinalis*, and *Bacteroides dorei*, as well as more aerobic and peritoneal species such as *Cutibacterium acnes* and *Staphylococcus capitis* (Figure 5E).[41,42] This indicated that LIFT-based bacterial single-cell omics could be applied to tissue samples to obtain high-quality genomes. The metabolic labeling of the peptidoglycan cell wall also highlighted the activity of these bacteria in the mouse colon.

We next applied LIFT to tumor samples from human patients. Resected tumor tissues from a patient diagnosed with colorectal cancer (Figure S9A) were cut into tissue sections and loaded onto the slide for microbial single-cell omics (Figure 6A). We confirmed cancer infiltration and staging by immunohistochemical staining of marker genes such as P53, BrafV600E, and Ki67 (Figure S9B). Using antibodies against bacterial lipopolysaccharide (LPS) and vancomycin to detect Gram-negative and Gram-positive bacteria, respectively, we observed microbes with diverse morphological features, including rod shape and spherical shape, distributed in colorectal cancer (Figure S9C). In this colorectal cancer tissue section, we searched for microbes in the bright field. The microbes have distinct Raman spectral fingerprints compared to the Raman spectra of the adjacent human cells (Figure S9D). This LIFT-based single-cell approach can thus effectively avoid sequencing of host cells or collection of non-microbial particles. For this colorectal cancer sample, a 1.33-μm-long and rod-shaped single cell was spotted and separated for genomic sequencing combined with Raman spectrum acquisition (Figures 6B and 6C). We obtained a medium-quality SAG identified as *Bacteroides intestinalis* based on Mash analysis (Figure 6D). Phylogenetic analysis of all *B. intestinalis* genomes from gut metadata of the Mash database and our SAG revealed that the SAG was similar to MGYG000028343, which has previously been observed in Chinese individuals (Figure 6E).[43]

A microbial single-cell transcriptome was also obtained from tissue samples. A rod-shaped single cell adhered to intestinal mucosa in the human colorectal cancer sample was separated for RNA sequencing (Figure 7A). After removal of host gene

(D) LIFT ejection of bacteria on mouse gut sections in fluorescent field. Bacteria outside (left) and inside (right) the tissue labeled with Fam-ADA were ejected by LIFT. Scale bar, 10 μm.

(E) 25 single bacteria were isolated from three fields of a single mouse gut section. A phylogeny constructed from 25 obtained SAGs is represented by the inner dendrogram (PhyloPhlAn, STAR Methods). The phylum of each SAG is indicated by the branch color. The completeness (purple) and contamination (green) of each SAG are represented by two heatmaps overlaid on the phylogenetic tree. The species name of each SAG is listed in the outermost ring.

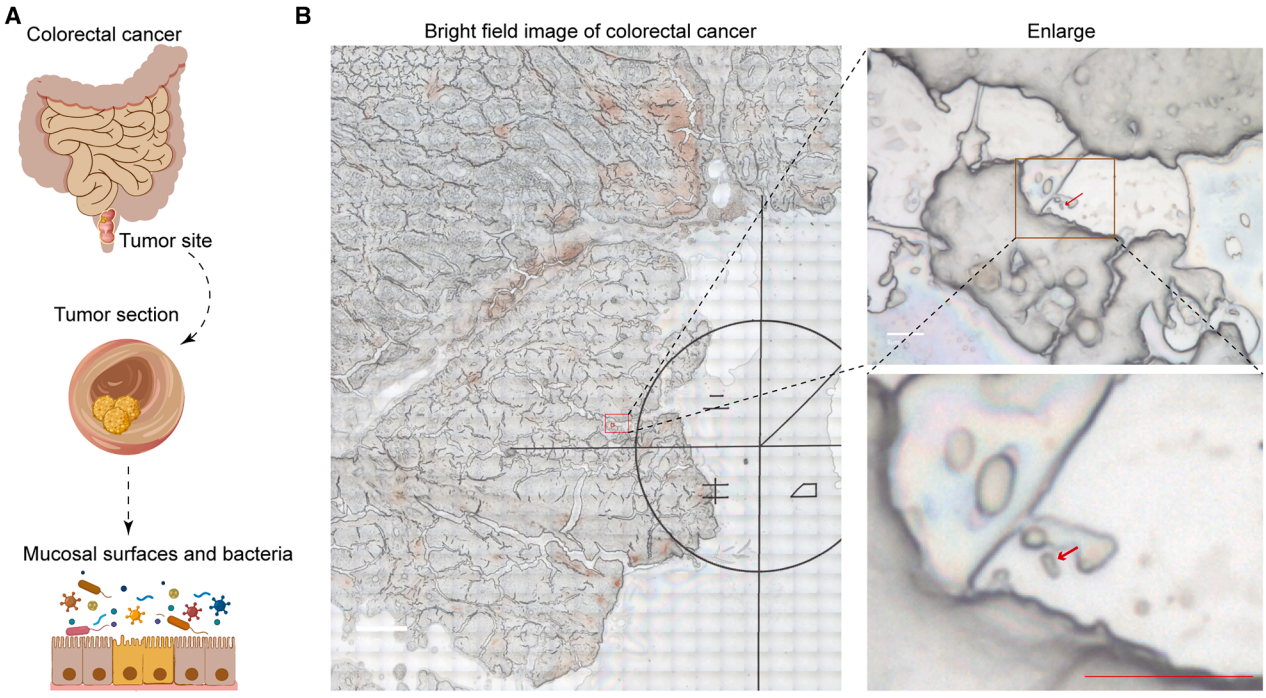

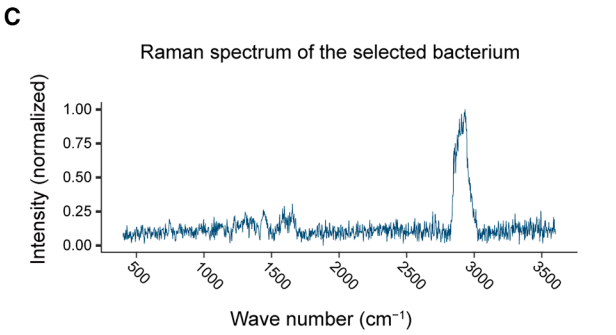

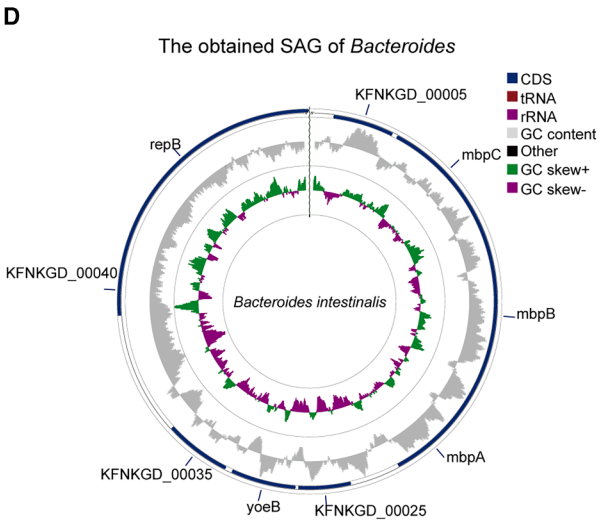

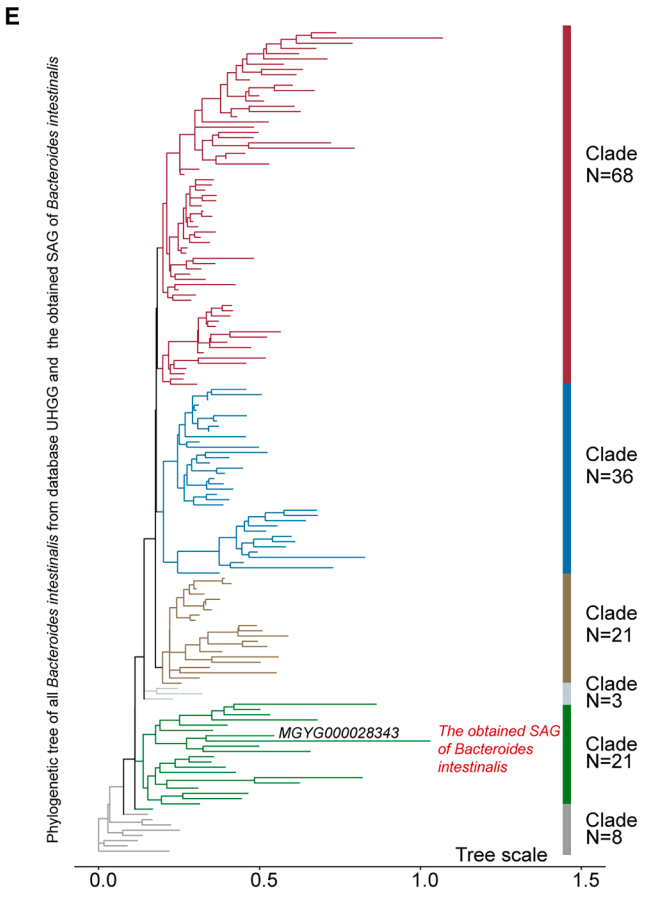

(legend on next page)

reads, we obtained a *de novo* transcriptome assembly identified as *Bacteroides xylanisolvens* according to the GTDB-Tk database (Figure 7B). The assembled single-cell transcriptome had 70% of the contigs and 75% of the transcripts (2,756 transcripts) belonging to *Bacteroides* (Figure 7B). *B. xylanisolvens* has been reported to be involved in nicotine degradation in smokers.[44] We found dust particles in the lungs of this patient with colorectal cancer, who has lung metastasis and a 50-year history of smoking (Figures S10A and S10B). Among the ~3,616 genes expressed by this *B. xylanisolvens* single cell were nicotine-degrading gene *nicX*, membrane protein *SusC/RagA* family TonB-linked outer membrane protein, ABC transporter, sialic-acid-specific acetylesterase, and porin (Figure 7C), which are crucial for nicotine degradation, crucial for nutrient uptake, and associated with the presence of *Bacteroidetes* in the gut.[45–47] GO analysis further verified that these genes were enriched in pathways of passive transmembrane transporter activity, sialic acid transmembrane transporter activity, and porin activity (Figure 7D), potentially damaging the gut environment. These results demonstrate the application of LIFT to obtain samples for reference-free analysis of tissue-resident microbes and to potentially apply it to single-cell spatial microbiome analyses.

DISCUSSION

Single-cell omics without droplets and long barcodes

Here, we establish a unified approach for high-quality microbial single-cell genomics or transcriptomics independent of droplet microfluidics. This LIFT-based method can precisely and automatically isolate individual bacteria from complex samples, in either a label-dependent or label-free manner. After rapid automated sorting, the cells were transferred to an automated platform for nucleic acid extraction and amplification, in preparation for subsequent single-cell genome or transcriptome sequencing to enhance throughput. In contrast to other single-cell methods for bacteria[48] (Table S5), we provide an *in situ* microbial single-cell omics method that enables the acquisition of high-quality microbial genomes and transcriptomes directly from complex samples. We are positive that further reduction of the reaction volumes (Figure S4C) and optimization of the reagents from lysis, random primers,[49] and MDA (Table S2; Figure S3H), optimization of the plasticware and developments in the precision selection process will further demonstrate the advantage of this single-cell omics approach that does not rely on microfluidics and exhaustive sequencing of abundant cells. As other microbial single-cell methods evolve,[49–51] our LIFT-based approach may also incorporate new developments. Without a requirement for complex barcodes, we currently maximize the effective read length from high-throughput sequencing. However, making full use of the positional information from our *in situ* method, potentially together with host tissue spatial transcriptome data, would likely require some barcode design.

scDNA and scRNA without prior knowledge of the microbes

Knowing the complete single-cell genome and transcriptome would be very useful to understanding fundamental questions of the microbiome beyond model organisms. Both the single-cell genome and the transcriptome could be either reference based or *de novo* assembled; the latter allows for samples that are not model bacterial species. Whereas mammalian genomes only contain about 20,000 genes, the total number of unique genes in their commensal microbes makes a much larger collective sum.[19] A recent application of multiplexed error-robust FISH (MERFISH) and expansion gel to bacterial cells required prior knowledge of the sequences for probe design[52] (Table S5). As is commonly seen for single-cell studies of mammalian cells, merely increasing the number of cells sequenced by a few-fold would not necessarily ensure identification of rare populations. With our approach, rare populations could be visually and spectrally profiled and enriched prior to sequencing. Moreover, our method provided multidimensional information for the study of microbial single cells, including bacterial shape, size, and Raman spectrum. Software provided along with the equipment by its manufacturer could be set to select for cell size, shape, area, etc. (Figure S5B). Further standardization and algorithm development for the single-cell Raman spectra would allow more precision in subspecies analyses.[53]

Host-associated microbiome *in situ*

Another major advantage of the LIFT-based single-cell approach is that complex samples require minimal pretreatment and can contain non-target molecules, particles, or other cells. Separating neighboring cells would also allow the study of cell-cell cooperation within a natural environment.

We have previously reported multiple *Bacteroides* species in an Austrian cohort of colorectal adenoma and carcinoma,[54,55] and *B. fragilis* is typically studied in mouse models of colitis.[56] Here, our scRNA analyses have tentatively identified bacterial metabolism of nicotine and mucin *in situ*. Further application of our microbial single-cell omics method to clinical samples may facilitate patient stratification and treatment.

Figure 6. Genomic sequencing for a single microbe in tissue

(A) Diagram for obtaining sections of the colorectal cancer sample.

(B) Isolating microbial single cells from colorectal cancer sections by LIFT. The enlarged image displays the ejected microbial single cell. The microbial single cell marked by the arrow was ejected for genome sequencing. Scale bar, 10 μm.

(C) Raman spectrum of the indicated single cell from (B).

(D) Visualization of the obtained SAG (*Bacteroides intestinalis*) by the CGView tool displaying GC skew (green or purple), feature labels (CDS, tRNA, rRNA), GC content (gray), divider rings, and tick density.

(E) Phylogenetic tree (PhyloPhlAn) was constructed with the obtained SAG (bin Bacteroides) and all *B. intestinalis* genomes downloaded from gut metadata of the UHGG database. Our SAG is closest to that of the *B. intestinalis* MGYG000028343 Mash database, which was isolated from China. The average nucleotide identity (ANI) was calculated by Skani.

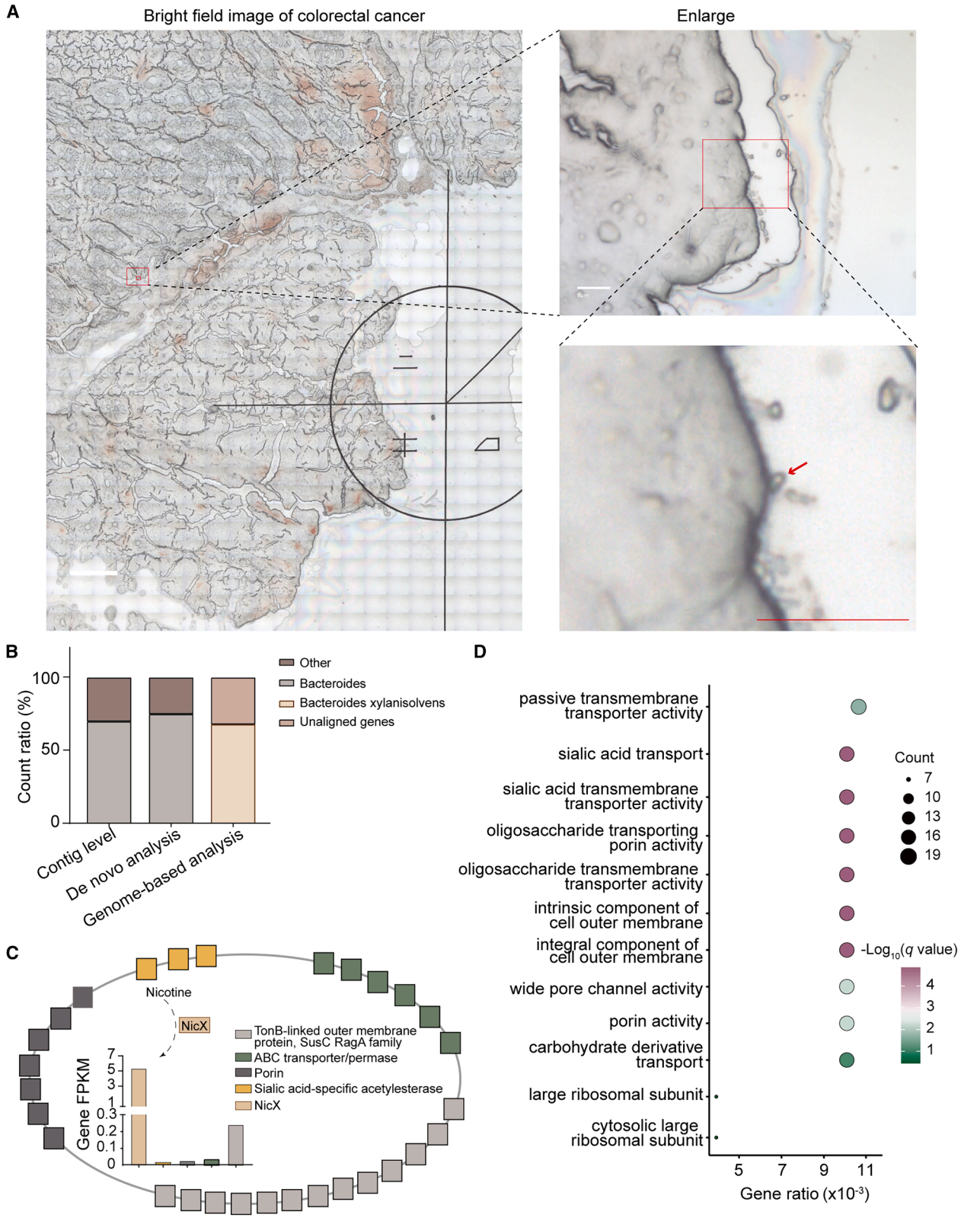

(legend on next page)

Limitations of the study

While we show the potential of this LIFT-, morphology-, and Raman-spectra-based microbial single-cell genomics and transcriptomics approach in a number of directions, the current study is a first step toward widespread applications. We have not tested a variety of human or mouse tissues or environmental samples other than soil. Labeling of the bacterial cells is optional, and other fluorescent or isotopic labels have not been tried. With the different compositions of the bacterial cell wall, the cell lysis procedure may need optimization for different samples (Figure S3J). The throughput and cost of this microbial single-cell method also need continued improvement, together with accumulating standard databases for the species- and subspecies-level single-cell morphology and Raman spectra. We have tentatively identified oligo(A) in a number of transcripts in citric-acid-induced sporulating *B. licheniformis* (Table S4), including oligo(A) in the full-length and partial mRNA for the citric acid transporter (Figure S7). RNA dynamics in such cases would require careful examination using other methods, and different bacterial species likely have different enzymes and different RNA half-lives. *In situ* gene expression would need to be investigated in complex microbial communities or host tissues to reveal more interesting biological stories.

In summary, we present an optics-based strategy for precision single-cell microbial genomes and transcriptomes that could fully capture the genomic landscape of host-associated microbiomes and allow nucleotide-resolution understanding of microbial gene transcription and turnover in individual cells in their native environment.

RESOURCE AVAILABILITY

Lead contact

Further information and requests for resources and reagents should be directed to and will be fulfilled by the lead contact, Huijue Jia (huijue_jia@fudan.edu.cn).

Materials availability

This study did not generate new unique reagents. The identifiers of all biological materials are listed in the STAR Methods.

Data and code availability

The sequencing data are available at the National Genomics Data Center (NGDC) with the accession number NGDC BioProject: PRJCA030563. The scripts describing the data analysis process are available at Zenodo, DOI: https://doi.org/10.5281/zenodo.17291315, and are mirrored on GitHub at https://github.com/MicrobeLab/microbial-sc-omics-in-situ.

ACKNOWLEDGMENTS

The authors are grateful to Z. Yang, J. Ma, X. Zhang, H. Li, and M. Lin for equipment support and P. Sun and M. Kuang for sequencing support. We thank Prof. H. Chen (Shanghai Institute of Materia Medica, Chinese Academy of Sciences) and Prof. X. Feng (Jilin University) for their suggestions on mouse gut microbiota labeling.

AUTHOR CONTRIBUTIONS

H.J. conceived the project and performed early experiments; X.L. developed and performed the experiments with assistance from J.W. and L.L.; X.L. and J.W. optimized sequencing library preparation; J.H. and X.Z. prepared tissue sections; X.L., Q.L., and R.G. performed the sequencing data analysis; H.J. and X.L. wrote the original manuscript; H.J. and G.Z. revised the manuscript; and H.J. supervised the study.

DECLARATION OF INTERESTS

The authors declare no competing interests.

STAR★METHODS

Detailed methods are provided in the online version of this paper and include the following:

- KEY RESOURCES TABLE
- EXPERIMENTAL MODEL AND STUDY PARTICIPANT DETAILS
  - Animals
  - Study participants and sample collection
- METHOD DETAILS
  - Laser-induced forward transfer (LIFT) of bacterial cells
  - Whole genome amplification and sequencing from single bacterial cells
  - Genome assembly and analyses
  - Whole transcriptome amplification and sequencing from single bacterial cells
  - Single-cell transcriptome analyses
  - *Bacillus licheniformis* culture and transmission electron microscopy
  - Metabolic labeling with fluorescent D-alanine in culture
  - Metabolic labeling with fluorescent D-alanine in mice
  - Tissue pretreatment for LIFT cell sorting and hematoxylin-eosin staining, immunofluorescence staining, and gomoris staining
- QUANTIFICATION AND STATISTICAL ANALYSIS

Figure 7. Transcriptome sequencing for a single microbe from tissue

(A) Tissue section was obtained as indicated in Figure 6. The enlarged image shows the ejected microbial single cell (marked by the arrow) for scRNA sequencing. Scale bar, 10 μm.

(B) Count ratio of contigs, transcripts in single-cell assembled transcriptomes, and genes by genome-based analysis for the bacterium shown in (A). The obtained single-cell assembled transcriptome was classified at a contig level using Kraken2, and the ratio of contigs belonging to the *Bacteroides* genus was calculated (total: 5,448). Transcript annotation was referred against the *de novo* transcriptome annotated by the eggNOG-mapper software, and the ratio of transcripts belonging to the *Bacteroides* genus was calculated (2,756 transcripts). Genome-based analysis was referred against the *Bacteroides xylanisolvens* genome (total: 5,306 genes), and the ratio of genes aligned to the *B. xylanisolvens* genome was calculated.

(C) The gene expression level of nicotine degradation gene *nicX* and proteins located on cell membrane. The oval ring denotes proteins in the cell membrane, including TonB-linked outer membrane protein (gray), ABC transporter/permease (dark green), porin (brown), and sialic acid acetylesterase (orange). The quantity of color-coded squares on the ring corresponds to the expression levels of the respective proteins. Gene FPKM was calculated by Bakta. For the plot inside the oval ring, the expression level of *NicX* was shown in the beige column, much higher than the membrane proteins.

(D) Gene Ontology analysis of transcripts classified to *Bacteroidetes*. The size of the dots indicates the number of genes enriched in each category, and the ratio in total is shown on the *y* axis. The color of the dots represents the log-transformed *q* value for each enriched category (green to magenta).

SUPPLEMENTAL INFORMATION

Supplemental information can be found online at https://doi.org/10.1016/j.xgen.2025.101128.

Received: May 23, 2025
Revised: August 16, 2025
Accepted: December 9, 2025
Published: January 22, 2026

REFERENCES

1. Stahl, P.L., Salmen, F., Vickovic, S., Lundmark, A., Navarro, J.F., Magnusson, J., Giacomello, S., Asp, M., Westholm, J.O., Huss, M., et al. (2016). Visualization and analysis of gene expression in tissue sections by spatial transcriptomics. Science *353*, 78–82. https://doi.org/10.1126/science.aaf2403.
2. Kuchina, A., Brettner, L.M., Paleologu, L., Roco, C.M., Rosenberg, A.B., Carignano, A., Kibler, R., Hirano, M., DePaolo, R.W., and Seelig, G. (2021). Microbial single-cell RNA sequencing by split-pool barcoding. Science *371*, eaba5257. https://doi.org/10.1126/science.aba5257.
3. Kashtan, N., Roggensack, S.E., Rodrigue, S., Thompson, J.W., Biller, S.J., Coe, A., Ding, H., Marttinen, P., Malmstrom, R.R., Stocker, R., et al. (2014). Single-cell genomics reveals hundreds of coexisting subpopulations in wild Prochlorococcus. Science *344*, 416–420. https://doi.org/10.1126/science.1248575.
4. Rinke, C., Schwientek, P., Sczyrba, A., Ivanova, N.N., Anderson, I.J., Cheng, J.F., Darling, A., Malfatti, S., Swan, B.K., Gies, E.A., et al. (2013). Insights into the phylogeny and coding potential of microbial dark matter. Nature *499*, 431–437. https://doi.org/10.1038/nature12352.
5. Zheng, W., Zhao, S., Yin, Y., Zhang, H., Needham, D.M., Evans, E.D., Dai, C.L., Lu, P.J., Alm, E.J., and Weitz, D.A. (2022). High-throughput, single-microbe genomics with strain resolution, applied to a human gut microbiome. Science *376*, eabm1483. https://doi.org/10.1126/science.abm1483.
6. Dar, D., Dar, N., Cai, L., and Newman, D.K. (2021). Spatial transcriptomics of planktonic and sessile bacterial populations at single-cell resolution. Science *373*, eabi4882. https://doi.org/10.1126/science.abi4882.
7. Pountain, A.W., Jiang, P., Yao, T., Homaee, E., Guan, Y., McDonald, K.J.C., Podkowik, M., Shopsin, B., Torres, V.J., Golding, I., and Yanai, I. (2024). Transcription-replication interactions reveal bacterial genome regulation. Nature *626*, 661–669. https://doi.org/10.1038/s41586-023-06974-w.
8. Lan, F., Saba, J., Ross, T.D., Zhou, Z., Krauska, K., Anantharaman, K., Landick, R., and Venturelli, O.S. (2024). Massively parallel single-cell sequencing of diverse microbial populations. Nat. Methods *21*, 228–235. https://doi.org/10.1038/s41592-023-02157-7.
9. Ma, P., Amemiya, H.M., He, L.L., Gandhi, S.J., Nicol, R., Bhattacharyya, R.P., Smillie, C.S., and Hung, D.T. (2023). Bacterial droplet-based single-cell RNA-seq reveals antibiotic-associated heterogeneous cellular states. Cell *186*, 877–891.e14. https://doi.org/10.1016/j.cell.2023.01.002.
10. Florian, C., and Serra, P. (2023). Printing via Laser-Induced Forward Transfer and the Future of Digital Manufacturing. Materials *16*, 698. https://doi.org/10.3390/ma16020698.
11. Barron, J.A., Krizman, D.B., and Ringeisen, B.R. (2005). Laser printing of single cells: statistical analysis, cell viability, and stress. Ann. Biomed. Eng. *33*, 121–130. https://doi.org/10.1007/s10439-005-8971-x.
12. Karakaidos, P., Kryou, C., Simigdala, N., Klinakis, A., and Zergioti, I. (2022). Laser Bioprinting of Cells Using UV and Visible Wavelengths: A Comparative DNA Damage Study. Bioengineering (Basel) *9*, 378. https://doi.org/10.3390/bioengineering9080378.
13. Kryou, C., and Zergioti, I. (2022). Laser-Induced Forward Transfer on Regenerative Medicine Applications. Biomedical Materials & Devices *1*, 5–20. https://doi.org/10.1007/s44174-022-00040-1.
14. Deng, Y., Renaud, P., Guo, Z., Huang, Z., and Chen, Y. (2017). Single cell isolation process with laser induced forward transfer. J. Biol. Eng. *11*, 2. https://doi.org/10.1186/s13036-016-0045-0.
15. Ye, K., Chang, W., Xu, J., Guo, Y., Qin, Q., Dang, K., Han, X., Zhu, X., Ge, Q., Cui, Q., et al. (2024). Spatial transcriptomic profiling of isolated microregions in tissue sections utilizing laser-induced forward transfer. PLoS One *19*, e0305977. https://doi.org/10.1371/journal.pone.0305977.
16. Jia H. (2022). Investigating Human Diseases with the Microbiome. (Elsevier, ed. 1st,2022, https://www.elsevier.com/books/investigating-human-diseases-with-the-microbiome/jia/978-0-323-91369-0).
17. Liang P. (梁鹏) (2022). 基于激光诱导向前转移的微生物单细胞弹射分选技术研究 (Research on ejecting isolation of single microbial cells based on laser induced forward transfer). PhD thesis. (Changchun Institute of Optics, Fine Mechanics and Physics, Chinese Academy of Sciences). www.doc88.com/p-59439607240272.html.
18. Meyer, F., Fritz, A., Deng, Z.L., Koslicki, D., Lesker, T.R., Gurevich, A., Robertson, G., Alser, M., Antipov, D., Beghini, F., et al. (2022). Critical Assessment of Metagenome Interpretation: the second round of challenges. Nat. Methods *19*, 429–440. https://doi.org/10.1038/s41592-022-01431-4.
19. Li, J., Jia, H., Cai, X., Zhong, H., Feng, Q., Sunagawa, S., Arumugam, M., Kultima, J.R., Prifti, E., Nielsen, T., et al. (2014). An integrated catalog of reference genes in the human gut microbiome. Nat. Biotechnol. *32*, 834–841. https://doi.org/10.1038/nbt.2942.
20. Zhu, J., Tian, L., Chen, P., Han, M., Song, L., Tong, X., Sun, X., Yang, F., Lin, Z., Liu, X., et al. (2022). Over 50,000 Metagenomically Assembled Draft Genomes for the Human Oral Microbiome Reveal New Taxa. Genom. Proteom. Bioinform. *20*, 246–259. https://doi.org/10.1016/j.gpb.2021.05.001.
21. Bowers, R.M., Kyrpides, N.C., Stepanauskas, R., Harmon-Smith, M., Doud, D., Reddy, T.B.K., Schulz, F., Jarett, J., Rivers, A.R., Eloe-Fadrosh, E.A., et al. (2017). Minimum information about a single amplified genome (MISAG) and a metagenome-assembled genome (MIMAG) of bacteria and archaea. Nat. Biotechnol. *35*, 725–731. https://doi.org/10.1038/nbt.3893.
22. Greene, R.A., and Slepecky, R.A. (1972). Minimal requirements for commitment to sporulation in Bacillus megaterium. J. Bacteriol. *111*, 557–565. https://doi.org/10.1128/jb.111.2.557-565.1972.
23. Schultz, D., Wolynes, P.G., Ben Jacob, E., and Onuchic, J.N. (2009). Deciding fate in adverse times: sporulation and competence in Bacillus subtilis. Proc. Natl. Acad. Sci. USA *106*, 21027–21034. https://doi.org/10.1073/pnas.0912185106.
24. Macklin, D.N., Ahn-Horst, T.A., Choi, H., Ruggero, N.A., Carrera, J., Mason, J.C., Sun, G., Agmon, E., DeFelice, M.M., Maayan, I., et al. (2020). Simultaneous cross-evaluation of heterogeneous E. coli datasets via mechanistic simulation. Science *369*, eaav3751. https://doi.org/10.1126/science.aav3751.
25. Bandyra, K.J., and Luisi, B.F. (2013). Licensing and due process in the turnover of bacterial RNA. RNA Biol. *10*, 627–635. https://doi.org/10.4161/rna.24393.
26. Gorelik, M.G., Yakhnin, H., Pannuri, A., Walker, A.C., Pourciau, C., Czyz, D., Romeo, T., and Babitzke, P. (2024). Multitier regulation of the E. coli extreme acid stress response by CsrA. J. Bacteriol. *206*, e0035423. https://doi.org/10.1128/jb.00354-23.
27. McCoy, J.G., Levin, E.J., and Zhou, M. (2015). Structural insight into the PTS sugar transporter EIIC. Biochim. Biophys. Acta *1850*, 577–585. https://doi.org/10.1016/j.bbagen.2014.03.013.
28. Levdikov, V.M., Barynin, V.V., Grebenko, A.I., Melik-Adamyan, W.R., Lamzin, V.S., and Wilson, K.S. (1998). The structure of SAICAR synthase: an enzyme in the de novo pathway of purine nucleotide biosynthesis. Structure *6*, 363–376. https://doi.org/10.1016/s0969-2126(98)00038-0.
29. Mom, J., Chouikha, I., Valette, O., Pieulle, L., and Pelicic, V. (2024). Systematic functional analysis of the Com pilus in Streptococcus

sanguinis: a minimalistic type 4 filament dedicated to DNA uptake in monoderm bacteria. mBio *15*, e0266723. https://doi.org/10.1128/mbio.02667-23.

30. Price, D.R.G., and Wilson, A.C.C. (2014). A substrate ambiguous enzyme facilitates genome reduction in an intracellular symbiont. BMC Biol. *12*, 110. https://doi.org/10.1186/s12915-014-0110-4.
31. Bruand, C., Farache, M., McGovern, S., Ehrlich, S.D., and Polard, P. (2001). DnaB, DnaD and DnaI proteins are components of the Bacillus subtilis replication restart primosome. Mol. Microbiol. *42*, 245–255. https://doi.org/10.1046/j.1365-2958.2001.02631.x.
32. Shingler, V. (1996). Signal sensing by sigma 54-dependent regulators: derepression as a control mechanism. Mol. Microbiol. *19*, 409–416. https://doi.org/10.1046/j.1365-2958.1996.388920.x.
33. Ramakrishnan, V. (2002). Ribosome structure and the mechanism of translation. Cell *108*, 557–572. https://doi.org/10.1016/s0092-8674(02)00619-0.
34. Liu, G.F., Wang, X.X., Su, H.Z., and Lu, G.T. (2021). Progress on the GntR family transcription regulators in bacteria. Yi Chuan *43*, 66–73. https://doi.org/10.16288/j.yczz.20-245.
35. Jack, D.L., Yang, N.M., and Saier, M.H., Jr. (2001). The drug/metabolite transporter superfamily. Eur. J. Biochem. *268*, 3620–3639. https://doi.org/10.1046/j.1432-1327.2001.02265.x.
36. Zhang, R., Abdel-Motaal, H., Zou, Q., Guo, S., Zheng, X., Wang, Y., Zhang, Z., Meng, L., Xu, T., and Jiang, J. (2020). A Novel MFS-MDR Transporter, MdrP, Employs D223 as a Key Determinant in the Na(+) Translocation Coupled to Norfloxacin Efflux. Front. Microbiol. *11*, 955. https://doi.org/10.3389/fmicb.2020.00955.
37. Egan, K., Field, D., Rea, M.C., Ross, R.P., Hill, C., and Cotter, P.D. (2016). Bacteriocins: Novel Solutions to Age Old Spore-Related Problems? Front. Microbiol. *7*, 461. https://doi.org/10.3389/fmicb.2016.00461.
38. Premasiri, W.R., Lee, J.C., Sauer-Budge, A., Théberge, R., Costello, C.E., and Ziegler, L.D. (2016). The biochemical origins of the surface-enhanced Raman spectra of bacteria: a metabolomics profiling by SERS. Anal. Bioanal. Chem. *408*, 4631–4647. https://doi.org/10.1007/s00216-016-9540-x.
39. Kaila, V.R.I., and Wikström, M. (2021). Architecture of bacterial respiratory chains. Nat. Rev. Microbiol. *19*, 319–330. https://doi.org/10.1038/s41579-020-00486-4.
40. Lin, L., Wu, Q., Song, J., Du, Y., Gao, J., Song, Y., Wang, W., and Yang, C. (2020). Revealing the in vivo growth and division patterns of mouse gut bacteria. Sci. Adv. *6*, eabb2531. https://doi.org/10.1126/sciadv.abb2531.
41. Xiao, L., Feng, Q., Liang, S., Sonne, S.B., Xia, Z., Qiu, X., Li, X., Long, H., Zhang, J., Zhang, D., et al. (2015). A catalog of the mouse gut metagenome. Nat. Biotechnol. *33*, 1103–1108. https://doi.org/10.1038/nbt.3353.
42. Liu, L., Zhao, Y., Yang, W., Fan, Y., Han, L., Sheng, J., Tian, Y., and Gao, X. (2025). Rotenone Induces Parkinsonism with Constipation Symptoms in Mice by Disrupting the Gut Microecosystem, Inhibiting the PI3K-AKT Signaling Pathway and Gastrointestinal Motility. Int. J. Mol. Sci. *26*, 2079. https://doi.org/10.3390/ijms26052079.
43. Almeida, A., Nayfach, S., Boland, M., Strozzi, F., Beracochea, M., Shi, Z.J., Pollard, K.S., Sakharova, E., Parks, D.H., Hugenholtz, P., et al. (2021). A unified catalog of 204,938 reference genomes from the human gut microbiome. Nat. Biotechnol. *39*, 105–114. https://doi.org/10.1038/s41587-020-0603-3.
44. Chen, B., Sun, L., Zeng, G., Shen, Z., Wang, K., Yin, L., Xu, F., Wang, P., Ding, Y., Nie, Q., et al. (2022). Gut bacteria alleviate smoking-related NASH by degrading gut nicotine. Nature *610*, 562–568. https://doi.org/10.1038/s41586-022-05299-4.
45. Robinson, L.S., Lewis, W.G., and Lewis, A.L. (2017). The sialate O-acetylesterase EstA from gut Bacteroidetes species enables sialidase-mediated cross-species foraging of 9-O-acetylated sialoglycans. J. Biol. Chem. *292*, 11861–11872. https://doi.org/10.1074/jbc.M116.769232.
46. Papamichail, D., and Delihas, N. (2006). Outer membrane protein genes and their small non-coding RNA regulator genes in Photorhabdus luminescens. Biol. Direct *1*, 12. https://doi.org/10.1186/1745-6150-1-12.
47. Hall, L.M.C., Fawell, S.C., Shi, X., Faray-Kele, M.C., Aduse-Opoku, J., Whiley, R.A., and Curtis, M.A. (2005). Sequence diversity and antigenic variation at the rag locus of Porphyromonas gingivalis. Infect. Immun. *73*, 4253–4262. https://doi.org/10.1128/IAI.73.7.4253-4262.2005.
48. Pountain, A.W., and Yanai, I. (2025). Dissecting microbial communities with single-cell transcriptome analysis. Science *389*, eadp6252. https://doi.org/10.1126/science.adp6252.
49. Shen, Y., Qian, Q., Ding, L., Qu, W., Zhang, T., Song, M., Huang, Y., Wang, M., Xu, Z., Chen, J., et al. (2025). High-throughput single-microbe RNA sequencing reveals adaptive state heterogeneity and host-phage activity associations in human gut microbiome. Protein Cell *16*, 211–226. https://doi.org/10.1093/procel/pwae027.
50. Xu, Z., Wang, Y., Cai, W., Chen, Y., and Wang, Y. (2025). Single microorganism RNA sequencing of microbiomes using smRandom-Seq. Nat. Protoc. *21*, 160–199. https://doi.org/10.1038/s41596-025-01181-5.
51. Jia, M., Zhu, S., Xue, M.Y., Chen, H., Xu, J., Song, M., Tang, Y., Liu, X., Tao, Y., Zhang, T., et al. (2024). Single-cell transcriptomics across 2,534 microbial species reveals functional heterogeneity in the rumen microbiome. Nat. Microbiol. *9*, 1884–1898. https://doi.org/10.1038/s41564-024-01723-9.
52. Sarfatis, A., Wang, Y., Twumasi-Ankrah, N., and Moffitt, J.R. (2025). Highly multiplexed spatial transcriptomics in bacteria. Science *387*, eadr0932. https://doi.org/10.1126/science.adr0932.
53. Liang, Q., Lan, X., Wu, J., Wei, W., Li, L., Tang, X., Zhao, G., Guo, R., and Jia, H. (2025). Precision culturomics enabled by unlabeled single-cell morphology and Raman spectra. bioRxiv. https://doi.org/10.1101/2025.06.27.661433.
54. Feng, Q., Liang, S., Jia, H., Stadlmayr, A., Tang, L., Lan, Z., Zhang, D., Xia, H., Xu, X., Jie, Z., et al. (2015). Gut microbiome development along the colorectal adenoma-carcinoma sequence. Nat. Commun. *6*, 6528. https://doi.org/10.1038/ncomms7528.
55. Wang, J., and Jia, H. (2016). Metagenome-wide association studies: fine-mining the microbiome. Nat. Rev. Microbiol. *14*, 508–522. https://doi.org/10.1038/nrmicro.2016.83.
56. Wong, C.C., and Yu, J. (2023). Gut microbiota in colorectal cancer development and therapy. Nat. Rev. Clin. Oncol. *20*, 429–452. https://doi.org/10.1038/s41571-023-00766-x.
57. Chen, S., Zhou, Y., Chen, Y., and Gu, J. (2018). fastp: an ultra-fast all-in-one FASTQ preprocessor. Bioinformatics *34*, i884–i890. https://doi.org/10.1093/bioinformatics/bty560.
58. Nurk, S., Meleshko, D., Korobeynikov, A., and Pevzner, P.A. (2017). metaSPAdes: a new versatile metagenomic assembler. Genome Res. *27*, 824–834. https://doi.org/10.1101/gr.213959.116.
59. Wood, D.E., Lu, J., and Langmead, B. (2019). Improved metagenomic analysis with Kraken 2. Genome Biol. *20*, 257. https://doi.org/10.1186/s13059-019-1891-0.
60. Tolstoganov, I., Kamenev, Y., Kruglikov, R., Ochkalova, S., and Korobeynikov, A. (2022). BinSPreader: Refine binning results for fuller MAG reconstruction. iScience *25*, 104770. https://doi.org/10.1016/j.isci.2022.104770.
61. Chklovski, A., Parks, D.H., Woodcroft, B.J., and Tyson, G.W. (2023). CheckM2: a rapid, scalable and accurate tool for assessing microbial genome quality using machine learning. Nat. Methods *20*, 1203–1212. https://doi.org/10.1038/s41592-023-01940-w.
62. Chaumeil, P.A., Mussig, A.J., Hugenholtz, P., and Parks, D.H. (2019). GTDB-Tk: a toolkit to classify genomes with the Genome Taxonomy Database. Bioinformatics *36*, 1925–1927. https://doi.org/10.1093/bioinformatics/btz848.
63. Asnicar, F., Thomas, A.M., Beghini, F., Mengoni, C., Manara, S., Manghi, P., Zhu, Q., Bolzan, M., Cumbo, F., May, U., et al. (2020). Precise

phylogenetic analysis of microbial isolates and genomes from metagenomes using PhyloPhlAn 3.0. Nat. Commun. *11*, 2500. https://doi.org/10.1038/s41467-020-16366-7.

64. Schwengers, O., Jelonek, L., Dieckmann, M.A., Beyvers, S., Blom, J., and Goesmann, A. (2021). Bakta: rapid and standardized annotation of bacterial genomes via alignment-free sequence identification. Microb. Genom. *7*, 000685. https://doi.org/10.1099/mgen.0.000685.

65. Langmead, B., Trapnell, C., Pop, M., and Salzberg, S.L. (2009). Ultrafast and memory-efficient alignment of short DNA sequences to the human genome. Genome Biol. *10*, R25. https://doi.org/10.1186/gb-2009-10-3-r25.

66. Cantalapiedra, C.P., Hernández-Plaza, A., Letunic, I., Bork, P., and Huerta-Cepas, J. (2021). eggNOG-mapper v2: Functional Annotation, Orthology Assignments, and Domain Prediction at the Metagenomic Scale. Mol. Biol. Evol. *38*, 5825–5829. https://doi.org/10.1093/molbev/msab293.

67. Aramaki, T., Blanc-Mathieu, R., Endo, H., Ohkubo, K., Kanehisa, M., Goto, S., and Ogata, H. (2020). KofamKOALA: KEGG Ortholog assignment based on profile HMM and adaptive score threshold. Bioinformatics *36*, 2251–2252. https://doi.org/10.1093/bioinformatics/btz859.

68. Gligorijevic, V., Renfrew, P.D., Kosciolek, T., Leman, J.K., Berenberg, D., Vatanen, T., Chandler, C., Taylor, B.C., Fisk, I.M., Vlamakis, H., et al. (2021). Structure-based protein function prediction using graph convolutional networks. Nat. Commun. *12*, 3168. https://doi.org/10.1038/s41467-021-23303-9.

69. Liao, Y., Smyth, G.K., and Shi, W. (2014). featureCounts: an efficient general purpose program for assigning sequence reads to genomic features. Bioinformatics *30*, 923–930. https://doi.org/10.1093/bioinformatics/btt656.

70. Ondov, B.D., Treangen, T.J., Melsted, P., Mallonee, A.B., Bergman, N.H., Koren, S., and Phillippy, A.M. (2016). Mash: fast genome and metagenome distance estimation using MinHash. Genome Biol. *17*, 132. https://doi.org/10.1186/s13059-016-0997-x.

71. Hooke Instruments Ltd. (2022). PRECI SCS-R300 Raman Single Cell Sorter. (available at https://en.hooke-instruments.com/ProductCenter/unicellular/2022-02-18/41.html).

STAR★METHODS

KEY RESOURCES TABLE

REAGENT or RESOURCE	SOURCE	IDENTIFIER
Antibodies		
FITC anti-LPS	Cloud-Clone	Cat# MAB526Ge22 ; RRID:AB_3075414
Anti-Vancomycin	Invitrogen	Cat# V34850 ; N/A (fluorescent conjugate, not an antibody)
anti-CK20	ZSGB-BIO	Cat# ZA-0574 ; RRID: AB_3720801
anti-CDX2	ZSGB-BIO	Cat# ZA-0520 ; RRID: AB_3720802
anti-Villin	ZSGB-BIO	Cat# ZA-0575 ; RRID: AB_3720803
anti-MSH2	ZSGB-BIO	Cat# ZA-0622 ; RRID: AB_3720804
anti-MSH6	ZSGB-BIO	Cat# ZM-0367 ; RRID: AB_3720805
anti-MLH1	ZSGB-BIO	Cat# ZM-0152 ; RRID: AB_3720806
anti-PMS2	ZSGB-BIO	Cat# ZA-0542 ; RRID: AB_3720807
anti-P53	ZSGB-BIO	Cat# ZM-0408 ; RRID:AB_3096232
anti-BrafV600E	Roche	Cat# 760-5095 ; RRID:AB_3676084
anti-Ki67	ZSGB-BIO	Cat# ZM-0166 ; RRID:AB_2890067
Chemicals		
TADA	GuoPing Pharmaceutical	GP122520-1
Cy5ADA	GuoPing Pharmaceutical	GP122520-2
FamADA	GuoPing Pharmaceutical	GP122520-3
Nucleic acid extraction		
REPLI-g WGA single cell kit	QIAGEN	Cat# 150345
REPLI-g WTA single cell kit	QIAGEN	Cat# 150065
RNase Inhibitor	Vazyme	Cat# R301-01
MetaPolyzyme	Invitrogen	Cat# MAC4L
Experimental models: Strains		
Bacillus licheniformis	This manuscript	Isolated from saliva (human)
Staphylococcus capitis	This manuscript	Isolated from tongue swab (human)
Streptococcus oralis	This manuscript	Isolated from saliva (human)
Lactobacillus plantarum	This manuscript	Isolated from tongue (human)
Akkermansia muciniphila	BioSci Strain Company	Cat# BAA835
Bacteroides xylanisolvens	This manuscript	Isolated from feces (human)
Clostridium butyricum	This manuscript	Isolated from feces (human)
Sphingomonas sp. 000797515	Hooke Instruments, Ltd., China	Sequencing validated (soil)
Software and algorithms		
Fastp (0.23.2)	Chen et al.[57]	https://github.com/OpenGene/fastp
metaSPAdes (3.13.0)	Nurk et al.[58]	https://github.com/ablab/spades/releases
Kraken2(2.0.7)	Wood et al.[59]	https://ccb.jhu.edu/software/kraken2/
BinSpreader	Almeida et al.[60]	cab.spbu.ru/software/binspreader
CheckM2 (v.1.0.2)	Chklovski et al.[61]	https://github.com/chklovski/CheckM2
GTDB-Tk (1.0.2)	Chaumeil et al.[62]	https://github.com/Ecogenomics/GTDBTk
PhyloPlAn (3.0.67)	Asnicar et al.[63]	https://github.com/biobakery/phylophlan
Bakta (1.8.1)	Schwengers et al.[64]	https://github.com/oschwengers/bakta
Bowtie2 (v.2.1.0)	Langmead et al.[65]	http://bowtie-bio.sourceforge.net/bowtie2/index.shtml
Eggnog-mapper (5.0.2)	Cantalapiedra et al.[66]	https://github.com/eggnogdb/eggnog-mapper
Kofamscan	Aramaki et al.[67]	https://github.com/takaram/kofam_scan
DeepFRI	Gligorijević et al.[68]	https://github.com/flatironinstitute/DeepFRI

(*Continued on next page*)

Continued

REAGENT or RESOURCE	SOURCE	IDENTIFIER
FeatureCounts (2.0.3)	Liao et al.[69]	https://sourceforge.net/projects/subread/files/subread-2.0.3/
Mash (2.0)	Treangen et al.[70]	https://github.com/marbl/Mash
Custom scripts for scDNA and scRNA data analyses	This study	https://github.com/MicrobeLab/microbial-sc-omics-in-situ, https://doi.org/10.5281/zenodo.17291315

EXPERIMENTAL MODEL AND STUDY PARTICIPANT DETAILS

Animals

Specific pathogen-free C57BL/6 mice (female, 8 weeks old) were purchased from BESTEST Biotechnology Co., Ltd (Zhuhai, China) and maintained in the laboratory Animal Center of Greater Bay Area Institute of Precision Medicine (Guangzhou, China). These mice were bred in a temperature-controlled environment (25°C, 12-h light/dark cycle) with free access to food and clean drinking water. All animal experiments were approved by the Animal Ethics Committee at Greater Bay Area Institute of Precision Medicine and were performed in accordance with guidelines approved by the Institutional Review Board of Fudan University.

Study participants and sample collection

All the human adults studied here were volunteers not known to have chronic diseases, and did not take antibiotics within the past three months. All healthy volunteers and the cancer patient had written informed consent. All the samples were self-collected into a sterile tube, and handed in for further processing on the same day. The study was approved by the Institutional Review Board of Fudan University. Tissue collection was approved by the Ethics Committee at The Affiliated Panyu Central Hospital of Guangzhou Medical University and was conducted following guidelines established by this committee.

METHOD DETAILS

Laser-induced forward transfer (LIFT) of bacterial cells

The equipment, PRECI SCS-R300 (Hooke Instruments, Ltd., China), equipped with 24 receivers was turned on and adjusted according to standards following the manufacturer's handbook (Video S1).[71] The optical setup is shown in Figure S1. The Laser used for LIFT was nanosecond single pulse laser with 532nm wavelength, 5ns pulse width and 3.4μJ energy, which could produce a single adjustable spot capable of ejecting 0.5–20μm microorganisms. Within 500nJ LIFT energy, the diameter of the LIFT ejection spot is linearly and positively correlated with the laser energy. The equation is:

$$y = 0.012x + 1.4$$

Where x is the LIFT energy (nJ) and y is spot diameter (μm). For complex shape and larger microbes (greater than 20μm), LIFT combined with beam shaping could successfully sort them. Laser for Raman spectral acquisition was continuous laser with a maximum laser power of 50mW, 532nm wavelength. The parameters of the laser for the acquisition of Raman spectra are set to 3mW, 3s. The focused spot of Raman spectra acquisition is theoretically calculated as 886nm diameter.

The obtained samples were diluted to 5 mL with PBS, filtered through 40μm cell strainers (if needed), and centrifuged at 600g to remove impurities and cell debris. The resulting supernatant was centrifuged at 12,000g for 3 min to collect bacterial pellets, The bacterial pellet was washed twice with nuclease-free ddH_2O (12,000g, 30s). resuspended in nuclease-free ddH2O. These pretreatment steps do not exceed 15 min 1-2μL filtered and washed samples were spotted onto a quartz slide coated with 25nm thickness of aluminum film (HSC24, Hooke Instruments, Ltd.), and sterile air-dried in the hood. The Hooke chip was designed to incorporate a thermal insulation structure to effectively protect the cell from heat-induced damage. Visually selected bacterial cells (the manufacturer's software) were LIFT-transferred into Ultraviolet (UV) pre-treated receiver (HSR04, Hooke Instruments, Ltd.) filled with 0.5-1μL PBS using a laser energy below 75nJ (exceeding the minimum energy required by most microbes), and then flipped into individual PCR tubes with brief spinning at 2000g (Yooning Mini-6K).

Whole genome amplification and sequencing from single bacterial cells

Genome amplification was performed according to kit instructions (REPLI-g single cell kit, #150345, QIAGEN). Briefly, following cell lysis at 65°C for 10 min, Multiple displacement amplification (MDA) was performed using the REPLI-g scDNA Polymerase at 30°C for 6 h. Sequencing libraries (PE150) were constructed without PCR, and sequenced on a DNBSEQ-T7 high-throughput sequencer (MGI).

After the cells were automatically LIFTed into the plate, a three-step program was set up to complete the genome extraction and amplification, in accordance with the instructions for the QIAGEN kit (#150345) and the Firefly instrument (Sptlabtech firefly). In step one, 7.0μL lysis buffer and PBS were pipetted to lyse the cells at 65°C for 10 min. After cell lysis, 3.0μL stop solution buffer was

pipetted to terminate the lysis reaction in Steptwo. In Step three, 40μL MDA reaction buffer was pipetted to finish DNA amplification at 30°C for 6 h.

Genome assembly and analyses

Quality control on paired-end sequencing reads of raw data was performed by fastp tool.[57] The filtered reads were assembled by metaSPAdes (parameters: –sc).[58] Based on binning information provided by Kraken2 (parameters: –gzip-compressed, –paired, –use-mpa-style),[59] the obtained assembled bins were processed with bin refinement using BinSpreader.[60] The quality of genome bins was analyzed by Checkm2[61] (parameters: checkm lineage_wf, checkm tetra, checkm dist_plot) and QUAST. GTDB-Tk (parameters: gtdbtk classify_wf, –extension fa; database version r207) was used to classify and taxonomically assign genome bins.[62] Phylogenetic trees were constructed by PhyloPhlAn (parameters: –diversity medium) tool.[63] The phylogenetic tree was constructed using the PhyloPhlan pipeline[63] with a supermatrix (supermatrix_aa.cfg) approach and maximum likelihood method, rooted at the midpoint. Robustness was assessed by generating alternative trees with varied alignment subsets and model parameters. Mash (parameters: bestMash.py 0.05; UHGG version v2.0) was used for rapid assessment of distances between genomes.[70] Genome annotation was generated by Bakta.[64] Average Nucleotide Identity (ANI) was calculated by Skani (parameters: skani dist -t, -r; threshold 0.95).

Whole transcriptome amplification and sequencing from single bacterial cells

Whole transcriptome amplification was performed according to kit instructions (REPLI-g WTA single cell kit, #150065, QIAGEN). Cells were lysed using a lysis buffer containing 7 μL PBS,4 μL lysis solution and 0.1 μL murine RNase Inhibitor (Vazyme, #R303-01) at 24°C for 5 min, followed by 95°C for 3 min. Genomic DNA was then removed with 2 μL gDNA Wipeout Buffer at 42°C for 10 min cDNA was synthesized from the RNA using 6 μL Reverse-transcription mix at 42°C for 60 min, then stopped at 95°C for 3 min 10 μL cell ligation mix was added to the cDNA synthesis reaction. The mixture is incubated at 24°C for 30 min. MDA were performed with extended reaction time for bacteria instead of mammalian cells, for 4 h for MDA. Sequencing libraries (PE150) were constructed without PCR, and sequenced on a DNBSEQ-T7 high-throughput sequencer (MGI).

Single-cell transcriptome analyses

For *de novo* transcriptome analysis, filtered reads of scRNA sequencing sample was assembled using rnaSPAdes (parameters: –sc).[58] Bakta[64] (parameters: -db) conducts a comprehensive annotation of assembled transcriptome and generated transcripts.faa. Transcripts.faa were further annotated by eggnog-mapper[66] (parameters: emapper.py, -m diamond) for gene function. KofamScan[67] (parameters: -f mapper) is used to annotate protein sequences with KEGG Orthology (KO). DeepFRI[68] (parameters: –fasta_fn, -ont mf/bp/cc/ec) is used to predict Enzyme Commission (EC) numbers and Gene Ontology (GO) terms for Bakta annotated genes.[64] Reads were aligned to genes using Bowtie2[65] (parameter: bowtie2 -x, –sensitive). Reads were aligned to proteins using Diamond (parameters: diamond blastx, –query, –sensitive).

For analyzing the distribution and characteristics of oligoA, bioawk tool is used to analyze oligoA positions in reads, geneand contig levelfrom Bakta annotation files. This process resulted in a matrix containing gene/contig lengths, oligoA positions, gene start and gene end positions. All transcripts in *de novo* transcriptome were evenly divided into ten percentile according to gene length. The number of occurrences of oligoA positions within each percentile range of the gene lengths was recorded. Standard deviation of oligoA distribution was calculated according to the fraction of counts in each percentile range of the gene length. The proportion of oligoA occurrence from each percentile was normalized by R package "Mfuzz". The analysis of poly(A) with nine adenylate residues (9A) or more followed these steps.

For genome-based analysis, Bowtie2 is used to align reads to transcripts and calculate gene FPKM values.[65] Reads are referred against *Bacillus licheniformis* genome and genome annotation GTF file (GCF_002074095.1) downloaded from NCBI database. After alignment with Bowtie2, gene quantification was performed using featureCount[69] (parameters: -t CDS -f -g gene_id). Genes expression with fold change $\geq$1.0 and p value < 0.05 were determined as significant change using R package DESeq2 (version 1.20.0). Gene enrichment of Biological Process (BP), Molecular Function (MF), Cell Component (CC) was analyzed by R package Clusterprofiler with p value Cutoff = 0.05. Heatmaps of gene expression were using R package "pheatmap". The bar plots, bubble plots of GO analysis, scatterplots, and boxplots were visualized using the on-line tool ImageGP (http://www.ehbio.com/ImageGP/index.php/Home/Index/index.html).

Bacillus licheniformis culture and transmission electron microscopy

The stored *Bacillus licheniformis* strain was inoculated into the Columbia Broth medium overnight at 37°C. 100μL *Bacillus licheniformis* suspension was transferred to 2mL medium containing 10% Columbia Broth, in which pH was adjusted to 4.0 by adding citric acid. *Bacillus licheniformis* were cultured in citric acid-amended 10% Columbia Broth for day 3 (exhibited a variety of morphologies) and day 9 (almost all transformed into spore at day 9). Then *Bacillus licheniformis* suspension was passed through 40μm cell strainers to eliminate cell clumps. The resulting filtrate was centrifuged at 12,000g for 3 min to collect bacterial pellets. These pellets were then washed three times with 1.5 mL of PBS each and finally resuspended in 0.7mL ddH2O. Prior to using PRECI SCS R300 devices, 1–2 μL of the cell suspension was dropped onto chip and allowed to dry either by evaporation at room temperature or by exposure to sterile airflow in a biosafety cabinet.

For transmission electron microscopy, citric acid treated *Bacillus licheniformis* were fixed with 4% PFA and stored at 4°C. The copper mesh was incubated in 10μL fixed *Bacillus licheniformis* solution for 2 min. After removal of excessive solution using filter paper, copper mesh was incubated with 1% phosphotungstic acid (PTA) for 2 min and observed by electron microscope (FEI Tecnai G2 spirit).

Metabolic labeling with fluorescent D-alanine in culture

TADA (tetramethylrhodamine-amino-D-alanine), Cy3ADA (Cyanine3-amino-D-alanine) and FamADA (5-Carboxyfluorescein-amino-D-alanine) were purchased from GuoPing Pharmaceutical (Anhui province, China). *Staphylococcus capitis*, *Streptococcus oralis*, *Lactobacillus plantarum*, *Akkermansia muciniphila* and *Clostridium butyricum* were isolated from feces and saliva using our LIFT technology and cultured in Gifu Anaerobic Medium at anaerobic incubator. The *Sphingomonas* sp*000797515* were generously provided by HOOKE Instruments Ltd. The *Sphingomonas* sp*000797515* were cultured in Luria-Bertani Medium and incubated with TADA probes (40mM) at 37°C for 3 h. After incubation, the *Sphingomonas* sp*000797515* were washed with PBS thrice, and mixed with other single-strain bacteria in ddH2O for the following analyses. The *Sphingomonas* sp*000797515* genome provided was assembled from our single strain suspension sequencing.

Metabolic labeling with fluorescent D-alanine in mice

Cy3ADA and FamADA were administered to mice via gavage to label mouse gut microbiota. In brief, Mice were gavaged with Cy3ADA and FamADA probes dissolved in 200μL of PBS at 1 mM concentration. 6 h later, Mice were anesthetized using sodium pentobarbital (50 mg/kg). A part of mouse large intestine was excised and minced using scissors in 2mL of PBS buffer. Subsequently, the minced tissue was passed through 40μm cell strainers to eliminate nonbacterial tissues and food debris. The resulting filtrate was centrifuged at 12,000g for 3 min to collect bacterial pellets. These pellets were then washed three times with 1.5mL of PBS each and finally resuspended in ddH2O. The bacterial suspension was placed under a Leica fluorescence microscope (ECLIPSE Ni-U) to observe the labeling of the bacteria.

Tissue pretreatment for LIFT cell sorting and hematoxylin-eosin staining, immunofluorescence staining, and gomoris staining

After euthanizing the mice, a small segment of colon tissue (0.5–0.8cm length) free of food debris was excised, embedded in OCT (optimal cutting temperature compound), and frozen. The frozen colon tissue was sectioned into slices with 6μm thickness and mounted flat onto glass slides and LIFT chip.

Several pieces of 2mm thickness tissues (20 × 20 × 2mm) separated by laparoscopic colorectal cancer surgery were placed on filter paper and dry gauze pad. After removal of excessive water, tissues were transferred to supporter of freezing microtome (Leica CM1860 UV) and embedded with OCT. In order to ensure the operation of the tissue section, OCT embedded tissue was placed on cryo-stage until it's a solid ice cube. Processed tissue was sectioned into 7μm thickness for Raman spectrometry and LIFT on PRECI SCS-R300 (Hooke Instruments, Ltd., China) with 75nJ laser energy.

Dehydrated and paraffin embedded tissues were cut into 5μm thickness and were stained with hematoxylin-eosin after de-paraffinization. For immunofluorescence staining, tissue sections were treated with antigen retrieval buffers, and then permeabilized and blocked by mixed solution of 0.3% Triton X-100 and 5% BSA for 1 h. Primary antibodies were used to incubate tissue sections overnight at 4°C. Phosphate Buffer Saline containing 0.1% Tween 20 (PBST) was used to wash tissue sections five times. Well-washed sections were carefully incubated with secondary antibodies for 1 h at room temperature. DAPI (4′,6-diamidino-2-phenylindole) diluted at PBS with concentration 1:1000 was used to cell nuclei staining. Immunofluorescence images were captured by Leica sp8 system. Antibodies and their working concentration have been listed in the key resources table: anti-CK20 (ZSGB-BIO, #ZA-0574, 1:200), CDX2 (ZSGB-BIO, #ZA-0520, 1:200), Villin (ZSGB-BIO, #ZA-0575, 1:300), MSH2 (ZSGB-BIO, #ZA-0622, 1:250), MSH6 (ZSGB-BIO, #ZM-0367, 1:250), MLH1 (ZSGB-BIO, #ZM-0152, 1:300), PMS2 (ZSGB-BIO, #ZA-0542, 1:200), P53 (ZSGB-BIO, #ZM-0408, 1:200), BrafV600E (Roche, #760–5095, 1:300), and Ki67 (ZSGB-BIO, #ZM-0166, 1:300), anti-LPS (Cloud-Clone, #MAB526Ge22, 1:150), anti-Vancomycin (Invitrogen, #V34850, 1:150).

Gomoris staining method followed the manufacturer's protocol (Baso diagnostics. Inc. Zhuhai. China, #BA4375A). Briefly, 5μm thickness paraffin tissue sections were brought to water via xylene and descending grades of ethanol for deparaffinization. Following nuclear staining by Weigert's Iron Hematoxylin, sections were placed in Solution A for 15 min. After rinsing off the stain with distilled water, sections were stained with Solution B. After dehydration with ethanol and clearing with xylene, sections were mounted with a resinous medium.

QUANTIFICATION AND STATISTICAL ANALYSIS

Statistical analyses were performed by GraphPad Prism. Data were presented as the means ± SE. Biological replicates and calculation method for the significance of differences between groups were indicated in figure legends.